Republic of Iraq
Ministry of Higher Education
And Scientific Research
University of Kerbala
College of Science
Department of Physics

Construction of the Flame Coating system for Preparing Biocompatible Layer of Calcium Phosphate Medical Implants

A Thesis
Submitted to the College of Science, University of Kerbala
In partial Fulfillment of the Requirements For the Degree of
Master In Physics

By
Nabaa Mohammed Abdul Raheem
B.Sc.2019

Supervised by

Prof. Dr. Mohammed Abdulhur
Prof. Dr. Fadhil K. Fuliful

2022 A.C.   **1443 A.H.**

بسم الله الرحمن الرحيم

(قالوا سبحانك لا علم لنا إلا

ما علمتنا إنك أنت العليم الحكيم)

صدق الله العلي العظيم

سورة البقرة (الآية 32)

1

Certificate

We certify that the preparation of this thesis, entitled "**Constructing the flame coating system for Preparing Biocompatible Layer of Calcium Phosphate Medical Implants**" was made under our supervision by (Nabaa Mohammed Abdul Raheem) at the Department of physics, College of the Science, University of Karbala in partial fulfillment of the requirements for the degree of Master of Science in Physics.
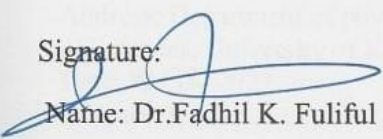
Signature:

Name: Dr. Mohammed A. Kadhim

Title: Professor

Address: Department of physics, College of Sciences, University of Kerbala
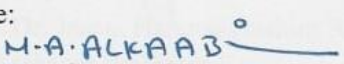
Date: 8 / 12 / 2022

Signature:

Name: Dr.Fadhil K. Fuliful

Title: Professor

Address: Department of physics, College of Sciences, University of Kerbala

Date: 8 / 12 / 2022

In view of the available recommendations, I forward this thesis for debate by the examining committee.

Signature:
M·A·ALKAAB

Name: Dr. Mohammed A. Alkaabi

Title: Assistant Professor

Head of Physics Department, College of Science

Date: 8 / 12 / 2022

Examination Committee Certification

We certify that we have read this thesis, entitled **" Constructing the flame coating system for Preparing Biocompatible Layer of Calcium Phosphate Medical Implants "** and as an examining committee, examined the student "**Nabaa Mohammed Abdul Raheem** "on its contents, and that in our opinion it is adequate for the partial fulfillment of the requirements for the degree of Master of Science in Physics.

Signature: *Bushra*

Name: Dr. Bushra A. Hasan
Title: Professor
Address: Department of physics, College of Sciences, University of Baghdad
(Chairman)
Date: 8 /12 / 2022

Signature:

Name: Dr. Nagham M. Kadhim
Title: Assistant Professor
Address: Department of physics, College of Sciences, University of Kerbala
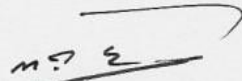Date: 12/ 12/ 2022
(Member)

Signature:

Name: Dr. Kadhim M. Kadhim
Title: Lecturer
Address: Department of physics, College of Sciences ,University of Kerbala
Date: 8 /12/2022
(Member)

Signature :

Name: Dr. Mohammed A. Kadhim
Title: Professor
Address: Department of physics, College of Sciences, University of Kerbala
(Supervisor)
Date: 8 /12 / 2022

Signature:

Name: Dr. Fadhil K. Fuliful
Title: Professor
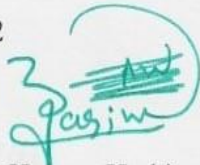Address: Department of physics, College of Sciences, University of Kerbala
(Supervisor)
Date: 8 /12 /2022

Signature:

Name: Dr. Jasem Hanoon Hashim Al-Awadi
Title: Assistant Professor
Dean of the College of Sciences, University of Kerbala
Date: 19/ 12/ 2022

Dedication

To…. The memory of My Father

To… My Mother

To.....My family

For those who supported me with their love, kindness

and encouragement

Nabaa

Acknowledgments

First of all , I thank God for helping me to complete this thesis ,and best prayers and peace on his best messenger Mohammed , his pure descendants and his noble companions. I would like to express my sincere appreciation and deep gratitude to my supervisors, Prof. Dr. Mohammed Abdulhur   and Prof. Dr. Fadhil K. Fuliful for suggesting the topic of this thesis, guidance, advice and continuous encouragement throughout the research.

My thanks go to all the staff members of the department of physics University of Karbala, I could hardly find any words to express my sincere gratitude to the staff of the laboratory of the department of physics.

I wish I had a better word than thanks for expressing my feelings to my father and mother for their patience and unlimited support with my brothers, sisters and friends for their prayers and kindness.

Nabaa

List of symbols

Symbols	Description	Units
d_{hkl}	Inter-planer distances	nm
FWHM	Full width at half maximum	Radian
$C.S$	Crystalline size	nm
H	Planck constant	J/s
I	Intensity	W/m^2
K	Wave vector	m^{-1}
X	Film thickness	nm
Θ	Diffraction angle	Degree
Λ	Wavelength	nm
β	Full width at half maximum of the diffraction	
n	Integer numbers	

List of Terms

Term	Description
SBF	Simulated Body Fluid Examination
$FTIR$	Fourier Transform Infrared Spectroscopy
$E.coli$	Escherichia coli
K $Pneumoniae$	Klebsiella Pneumoniae
$S.\ aureus$	Staphylococcus Aureus
$P.Aeruginosa$	Pseudomonas aeruginosa
$FE\text{-}SEM$	Field Emission Scanning Electron Microscopy
XRD	X-ray Diffraction

Abstract

In this work, a biocompatible layer of calcium phosphite was prepared on stainless steel substrates and tested for use as medical implants with layers compatible with in human body. These coatings have shorten the healing period for bone building on the materials used. The flame coating system was built and designed. Also, the properties of the deposited films were controlled by several variables (the ratio between the components, the distance between the flame source and the bases), the examination of the deposited films using several techniques. X-ray diffraction (XRD), infrared spectroscopy (FTIR), field emission scanning electron microscopy (FE-SEM) , X-ray energy dispersive spectrometry (EDX), then testing the deposited layers by immersing them in a solution simulating the human body to monitor the growth of the Hydroxyapatite (HA) layers on the deposited films to study the antibacterial activity of the prepared layers.

In this research, layers of calcium phosphite with different ratios (1.4, 1.5, 1.65, 1.8, 1.9) and different distances from the flame nozzle (2,3,4,5,6 cm) were prepared using the flame coating process on the substrate at a distance of 3 cm from flame nozzle. XRD showed many peaks that match the crystal structure of calcium phosphate. Additional peaks for the stainless steel substrate appeared in all samples. There are small differences in the positions of the peaks due to lattice strain due to the variation in crystal size. It is also clear that the intensity of the peaks increased at the ratio 1.65 and the best at the distance of 3 cm. On the other hand, the width of the peaks for the same sample decreases indicating higher crystallization level and crystal size growth.

Infrared spectroscopic examinations(FTIR) showed that the samples contained carbonate ions with bands showing at 1412.42, 1082.69 and 805.81 cm^{-1} for the organic compounds of the which gas butane used in the deposition process. In

addition, the hydroxide bands appeared in 3400, 1640.69, 6450.17 cm-1, which are identical to the water molecules adsorbed on the surface of the samples. It was demonstrated that the carbonate bands are of higher density compared to the phosphate bands indicating a high percentage of carbonates in all samples. Phosphate peaks were the most visible in the prepared sample with a ratio of 1.65 and a distance of 3 cm compared to the other samples.

Electron microscopy (FE-SEM) examination showed that the distinct and clear sample at the ratio of 1.65 and a distance of 3 cm, which has high porosity and contains distinct nanostructures.

The elements were analyzed using an energy-dispersive X-ray spectrometer (EDX) and the appearance of the basic elements for the synthesis of calcium phosphate. The samples were immersed in the body fluid simulating the human body to examine the biocompatibility, where the tests showed that the calcium phosphate ratio of 1.65 is the appropriate and biocompatible ratio in the human body. Tests showed antibacterial activity using diffusion disc technology. On the surface of the culture medium, was noticed the spread of Escherichia coli bacteria on the entire medium except for some areas around some samples.

The used method can be considered as a promising method to be used in coating medical implants in a simple way instead of the complicated traditional methods that require high technologies.

Contents

C H A P T E R   O N E

INTRODUCTION AND BASIC CONCEPTS

1.1 Introduction

Thin films play an important role in all fields of science and technology. Thin films do not change the properties of the material. The optical, electrical and thermal properties of the surface and the substrate can be completely changed [1].

Thin films have been used in many devices and applications such as solar cells, detectors, and many other devices. Where there is a wide demand for processing and developing biomaterials, modification of the selected biological and mechanical surface properties of biomaterials tends to be less time consuming. Thin coatings are a common technology. In surface engineering and modification, thin films deposition methods can be divided into chemical and physical. The chemical methods include sol-gel chemical reactions in the gas phase, while the physical methods include evaporation and spraying [2].

Thin material should be non-toxic to the tissues and cells of the body. Biomaterials films can be applied in medical applications, such as in bones, where thin films can be coated with biological materials for dental implants, orthopedics, and materials that mimic the human body, in addition to methods for modifying the skeletal surface structure of teeth [3].

Coatings are used in many medical and biological applications and contribute to a protective function or lead to a clear change in performance and function, especially when the substrate does not provide all the required properties [4].

The field of application of thin films in biomedicine is extensively applied because the surface of the material gives properties such as anti-bacterial, improving adhesion, and the strength of the immune reaction of the organism [5].

1.2 Thin films deposition methods

Physics has many branches, including solid state physics of several types, where we study thin films dealing with thicknesses from micrometers to nanometers. Thin films are deposited on solid materials such as silicon, polymers, and glass [6].

Thin films preparation methods are classified into two categories: physical methods and chemical methods, and they have proven their importance in effective techniques for thin film deposition, where a wide variety of techniques are designed as shown in Figure (1-1).

Thin films play a role in studying semiconductor compounds and materials in detail, providing fascinating information about their chemical, physical and synthetic properties [7]. It has many applications, including:

- **Electronic applications**

These applications are used in electronics and give high efficiency such as capacitors, digital circuits, etc. [8].

- **Optical applications**

These applications are used in the field of printers, filters and imaging, as well as in lenses and lenses of some wavelengths for use in solar cells or photovoltaic cells and reagents in general [9].
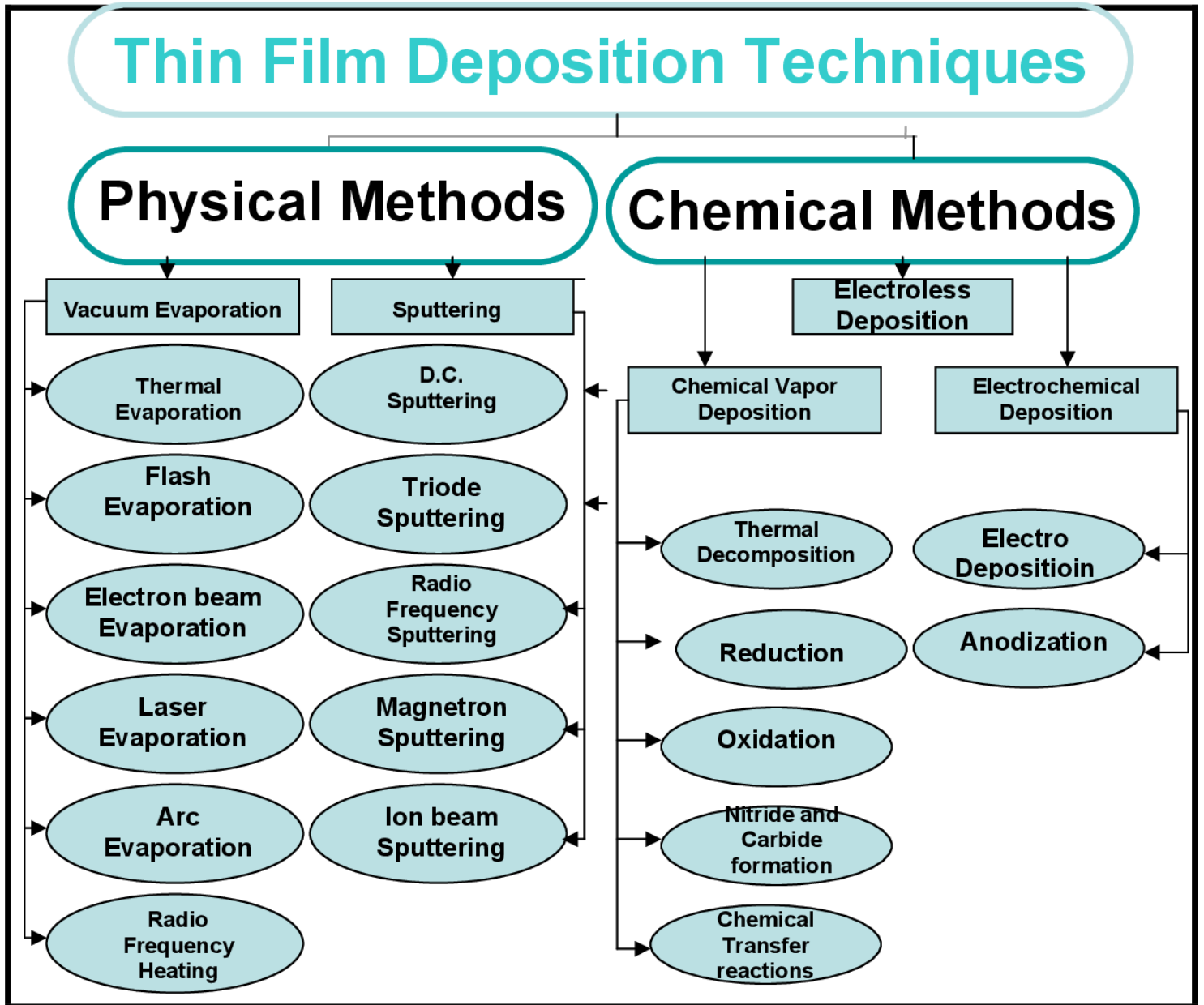
Figure 1.1: Thin films deposition methods [10]

1.3 Biomaterials

Biomaterials history Year Development Late 18 th – 19 th are man-made materials that are compatible with body tissues and classified into ceramics, polymers and composite materials, as well as they can be classified into natural or synthetic, and it is considered the most used technology in implants [11]. Biomaterials have been used to replace a part or function in the body in a safe and acceptable manner [12].

They are used in treatment and diseases and include common items such as sutures, needles, catheters, plates, dental fillings, etc. [13, 14]. Which can be used at any time period, as a whole or as part of a regimen that treats, strengthens or replaces any tissue, organ or function in the body [15].

The role of biomaterials has been greatly influenced by advances in many areas of biotechnology and the implant is an inaccessible area of the body's immune cells. It is also the first successful implantation process that uses biomaterials in dental implants and prosthetics. Biomaterials are used to manufacture drug-delivery implants. It is also used in the manufacture of pharmaceutical forms such as tablets and capsules [16]. It is used to develop implants in the body that interact with living tissues, and it is important in reducing the risks to which the patient is exposed and depends on several factors such as the chemical and physical nature of its components, the types of patient's tissues that are exposed to the device and the duration of that exposure. It is used as a supportive element to improve and prolong the patient's life, taking into account some factors, in-body contact (a tongue depressor can be used for a few seconds),optical properties (used in the eyes, skin, or teeth), appropriate mechanical properties (strength, stiffness, and fatigue properties)[17].

Biocompatibility is the ability of a substance to perform with an appropriate host response in a particular application, and it plays an important role because the patient is alive, so it must be biocompatible, a word widely used in biomaterials when incorporating any substance into the body without any immune responses called Biocompatible [18].
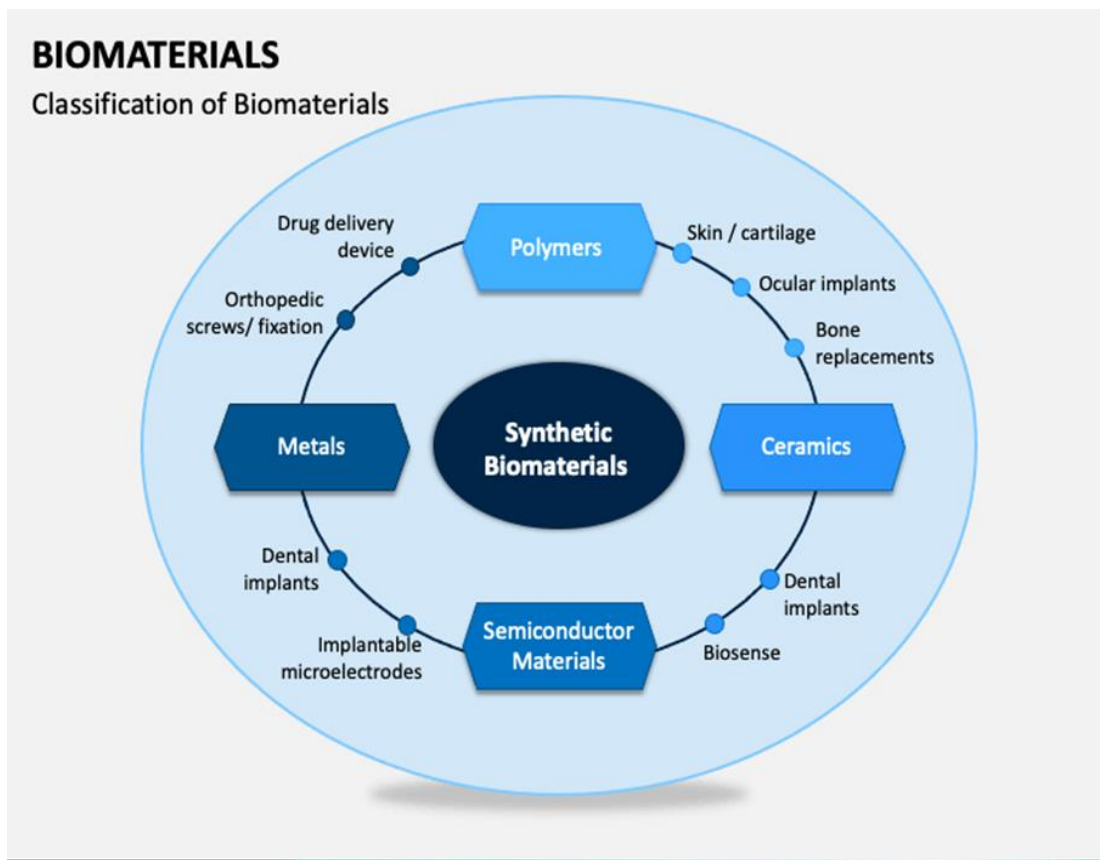
Figure 1.2: Classification of Biomaterials [19]

1.3.1 Classification of Biomaterials

Various classifications of biological materials are made on a wide scale, including:

- **Metal**

Metals are used almost exclusively in implants and in the knee and hip joints, as well as parts of metals are used in artificial heart valves. The uses of metal are wide, contributing to improving the properties of materials such as strength and resistance to corrosion, and steel is considered one of the most important metals used as a vital material. Viability, corrosion resistance, and mechanical properties. The advantages of using metals are that they are strong and resistant to fatigue and can be easily sterilized before use. As for the disadvantages of using metals, the metal can be corroded due to a chemical reaction with the body's enzymes and acids, and it can also cause toxicity of metal ions in the body [20].

- **Polymers**

They are the most widely used materials in medical and biological applications, and they are the preferred materials for blood vessels, as well as to replace and increase tissues. One of the advantages of using polymers is that they can be easily manufactured and modified, and their drawbacks are that important nutrients and water can be absorbed from the blood [21].

- **Ceramic**

Ceramics are used as components for hip and middle ear implants, as well as dental implants. One of the advantages of using ceramics is that it is strong and has high pressure that helps implant bone, and one of its disadvantages is that it is difficult to manufacture, and the implants can decompose from their place [22].

- **Inert biological materials**

The term "bio-inert" is applied to any material that is placed in the human body and does not chemically interact with tissues. Inert implants may be formed whose function depends on their integration in the implant, and examples of stainless steel [23].

- **Biomaterials biologically active**

Any substance that interacts with tissues inside the body is called "biologically active." When implants interact with tissues, body fluids produce a layer called apatite, which is biologically active. The main examples of these substances are hydroxyapatite [24].

- **Compound biomaterials**

It is important that every component of the composite is biocompatible as natural materials such as bone are viewed as composites some applications of composites in biomaterials applications are: (1) dental filling compounds, (2) bone cements (3) orthopedic implants with porous surfaces [25].

1.3.2 Properties of Biomaterials

The basic properties that a biomaterial must possess [26, 27]:

- ## Mechanical properties

Stress protection can be prevented by matching the modulus of elasticity from biomaterials to those in bone, which range from 4 to 30 GPA. Additionally, the materials should have a low modulus coupled with high strength to prolong implant service life and prevent laxity, thus preventing the need for revision surgery [26].

- **Biocompatibility**

   The materials developed must be compatible with living systems, not the cause harm any physical harm, which includes all the negative effects that a substance can have on its components Biological system [26].

- **High wear resistance**

   The material must have high wear resistance and exhibit low friction when sliding on body tissues. An increase or decrease in the coefficient of friction in abrasion resistance can lead to loosening of the implant [27].

- **Bone fusion:**

   For the first time, Osseo integration was defined as "the relationship between an arranged living bone and the bearing surface of the implant". Surface roughness, chemistry, and topography play a major role in bony fusion. Implant disassembly results from a lack of integration of the implant surface into the adjacent bone. A few researchers state that Osseo integration is not desirable due to the risk of not being able to remove the implant after use. However, a few of them have also shown that the implant can be removed safely. Thus, Osseo integration is desirable   the material is especially a vital material in some applications such as implants, where this must be ensured the implant will integrate properly with bone and other tissues [27].

- **Non-toxic**

   The material must not be genotoxic (which can alter the DNA of the genome) nor cytotoxic (cause damage to individual cell) [26].

1.4 Dental applications of biomaterials

Dental materials have always been essential, effective components of dental work but most restorations need to be replaced in time, Dental treatment often involves the placement of restorative materials or prepared dental implants. The introduction of an adhesive should improve results. The binding of vital materials to tissues and organs is very important in hardware application to support normal organ function. Teeth and gum tissues are exposed to damage and diseases due to the bacteria that controls them. Teeth or part of the teeth can be replaced and restored by a group of materials called biomaterials [28].
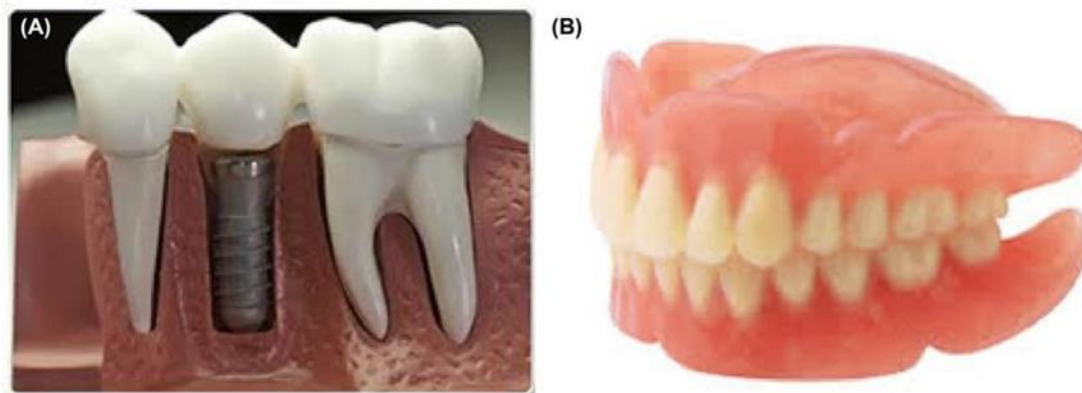
Figure 1.3: Dental applications of biomaterials (A) the endosteal root form dental implant and (B) biomaterial tooth gums. [28]

Dental implants can be inserted into the sites of the healed bone 3 months after [29].

Dental implants are used to replace missing teeth, and the dental implant process is considered successful because the implant simply works in the mouth. Success depends on the condition of the tissues surrounding the

implant and the teeth in addition to the comfort and satisfaction of patients [30].

1.5 Fundamentals of Medical Implant Materials

1.5.1 Implant Properties

Implants can be classified into important features [31]:

1- The human body must be compatible with the materials used, while there must be a tissue reaction due to the introduction of a foreign substance, which leads to chemical and physical changes, but does not affect the equipment.

2-The implant must have a required balance of mechanical and physical properties such as stress, flexibility, ductility, resistance to abrasion, etc.

3- The device must be easy, repeatable, and compatible with all biological requirements and techniques.

1.5.2 Implant Failure

From the time the implant was inserted into the body there are four different types of tissue [32]:

1. The substance is toxic, and tissues will die around it

2. The material is non-toxic, biologically inactive, fibrous tissue is formed

3. The material is non-toxic and active, and the tissue bonds with it

4. The material is non-toxic and melts, and the surrounding tissue replaces it

The planting material, its architecture and the environmental conditions around it play a very important role. There are reasons that lead to implant rejection, for example, improper healing (slow tissue growth), or wearing or breaking implants may lead to the formation of some unsuitable effects, or the deterioration of materials due to interaction between enzymes [33].

1.5.3 Bone healing/repair around implants

The process of bone repair begins when the implant is inserted into the operations that take place on the implant, where fracture healing is regulated by factors that affect cells and the response is according to fracture healing [34] and that the calcium phosphate coatings are the only ones that have the properties of conducting bone, and the biological activity of the surface can be checked by a solution that simulates the human body after the incubation period, where Hydroxyapatite (HA) is formed and after this period we notice that the coatings have a high degree of biological activity [35].

1.6 Metallic Implants (Stainless steel)

Among the first bio-metallic materials used in the manufacture of orthopedic implants was stainless steel, which appeared on the market in the 1920s and was considered superior to other available alloys due to its high resistance to corrosion. The most commonly used type of stainless steel is 316L stainless steel. Stainless steels have been used successfully for decades [36].

Stainless steel is considered a viable implant due to its availability and ease of handling [37], however, due to its limited strength, implants have been limited to certain parts, and dental crowns, and bridges and internal dental implants, stronger and more wear-resistant than the rapid development of medical devices. He added to the idea of medical devices and one of these metals is stainless steel 316L [38]. Type 316L stainless steel is an engineering material that is widely used nowadays because of its many corrosion features, high hardness, strength and cost in the market and poor anti-friction properties It has attracted much attention in the past decades and its hardness is up to 6.2

GPa and 316L samples have been tested and verified with regard to its structural and microstructural properties [39].

316L stainless steel (SS) has been used for a long time as bio-mineral materials as well as for orthopedic implants to make artificial joints, metal plates, screws, biocompatibility, excellent mechanical properties and reasonable cost [40]. One of the main materials that are used as implants, stainless steel is affected by many factors that affect the surface of the implant [41, 42].

Where the metal is dissolved in a soluble solution where we notice how the corrosion behavior is affected and there it must be taken into account the bio-implantable materials, the integrity of the implant and the adhesion of the implant to the bone and that the substrate is the main requirement in Osseo integration [43].

Metals are used in biomedicine. The choice of metal depends on its biocompatibility with body tissues, and the most widely used is stainless steel 316, although it is limited to the healing of bones, fractures and screws for fixation, and its manufacture is much easier than titanium, stainless steel is an iron-based alloy that contains carbon (C max 0.03%), chromium (chromium at least 16%) and nickel (nickel at least 10%) [44].

1.6.1 Bio Applications (Stainless steel)

Due to its high corrosive resistance and hardness with good mechanical properties and reasonable cost, the use of stainless steel (SS) 316 as medical implants [45, 46] these applications include orthopedic devices, orthodontic screws, and fracture repair. Corrosion in vital applications is an important part of what causes inflammatory reactions, and all of these factors affect the life of the implant and any failure leads to severe pain and postoperative operations

[47]. The study showed that the thin film formed by SS is more stable in biological applications and has an improved ability to adhere to cells [48].

1.6.2 Orthopedic Implants (Stainless steel)

Implants are used to stabilize fractures and joints, correct deformities, and many other applications. They provide mechanical stability to the bone through which bone function can be maintained and contribute to relieving pain. The implants have a relationship with bone healing [49].

Bone implants must provide biocompatibility with bone tissue and aim to restore bone function. Bone implants consist of bone implants that include various artificial joints (hip, knee, shoulder, and elbow) and orthopedic synthetic materials (wires, screws, screws, plates). Where different biomaterials were designed for bone implants, bone implants have undergone continuous development to improve their interactions with bone and ensure a successful problem for patients [50].

Stainless steel is the first metal to be used successfully as biomedical implants due to its excellent corrosion resistance [51, 52].

Metal materials are widely used as medical devices in cardiology, blood vessels, dentistry, and prosthetics. They are suitable for fixing bones and at the same time are easy to manufacture and formable [53] [54].

Figure 1.4: Stainless Steel Dental Crown [55]

1.7 Hydroxyapatite

The applications of daily biomaterials and metallic devices are being expanded, and they have been developed at the highest levels in orthopedic implants and replacements because they possess high strength [56].

Biocompatible coatings are applied to minerals. Hydroxyapatite is a biologically active, biocompatible coating that is very similar to bone and is able to form a strong bond between the implant and the bone [57, 58].

The introduction of hydroxyapatite is an important milestone in implant stabilization and the longevity of the implant in the human body, and its vital activity has been proven in many studies and allows a quick transfer between the two components, and early mobilization for the patient, which leads to a faster performance and is widely used in medical applications [59]. Plasma spray is the most common method for hydroxyapatite coatings.

1.7.1 Hydroxyapatite $Ca_3(Po_4)_2$ in simulated body fluid

Hydroxyapatite is one of the main components of calcium phosphate because of its strong activity and biocompatibility. It enhances the adhesion

between the bone and the implant by forming an appetite layer. It is also used for implants [60].

The fluid simulating the human body is prepared by adding reagents in distilled water until a concentration ion is added to it, ensuring the total solubility of the reagent. The biomaterial is examined by several assays x-rays (XRD), infrared spectroscopy (FTIR), and scanning electron microscopy (SEM) [61].

Where samples are immersed in a solution that mimics the human body for a period ranging from 30 days to 56 days at room temperature precipitation of calcium phosphate in such biological solutions provides a way to create calcium phosphate coatings in 1987 The use of simulated body fluid SBF was tested in biological activity and the benefit of the mimic solution to the human body is its ability On the bonding of apatite with bone and when apatite is formed in the living body, where it multiplies in a liquid simulating a human with ionic concentrations equivalent to those found in human blood and that the biologically active substance is the one on which bone-like hydroxyapatite is formed after immersion in a liquid mimicking the body [62].

Where the coatings are produced by immersing the implant in an aqueous solution that produces apatite at a low temperature, it produces thin coatings that cover the entire implant, but at high temperature a strong bonding coating is formed [63].

1.7.2 Hydroxyapatite Powder

The basic material for each thermal spraying process is hydroxyapatite, where quantities of calcium and phosphate are mixed to produce hydroxyapatite. The ratio of calcium to phosphate is about 1.66 or

1.67. The quality of the coating depends on the form of plasma spray powders. The particles shaw a higher degree than the formed inside the plasma flame due to its larger surface area to the ratio its size [64].

1.8 Factors affecting coating loss

There are several factors that lead to the loss of calcium phosphate coating, including mechanical, factory-related factors, biological factors, or paint-related factors such as paint type and biological activity, where these factors interact with each other and lead to coating loss [65].

1.8.1 Implant-Related Factors

The design of the synthetic component may affect coating loss due to micro-motion or other factors such as corrosion accelerating coating loss and body corrosion. Additionally, fluid flow and pressure along the unstable implant all lead to coating loss [66].

The length of the implant affects the implant, there is a short and there is a long. The researcher [67] noticed that the short implant with a length of less than 10 mm caused implant failure, and the success rate was low (85.3%) when placing the implant in a place with a limited area or narrow (non-size). These factors affect the performance of the implant and lead to the failure of the connection between the bone and the implant. Also, the width of the implant affects early implantation failure. Implants that are narrower by 4 mm [68].

Implant failure can be divided into early or late failures, depending on when they occur. Early implant failure results from the inability to establish an intimate connection from the bone to the implant. This means that bone healing after implant insertion is poor or compromised which is characterized by poor

quality and quantity of bone. Thus, these factors may explain the higher failure rate [69].

The failure or malfunction of the medical implant is considered an important matter and is attributed to complex factors as in Figure (1-5). Bacteria can settle on the surface of medical implants during the implantation process, or later [70, 71] putting the performance and longevity of implants at risk. Furthermore, due to tissue damage surrounding the implant during the implantation procedure, immune responses in interphase to implant tissues are dysregulated, making the implant semi-implanted and an area more susceptible to infection. These factors make the treatment of antibiotic-associated infections very complex.
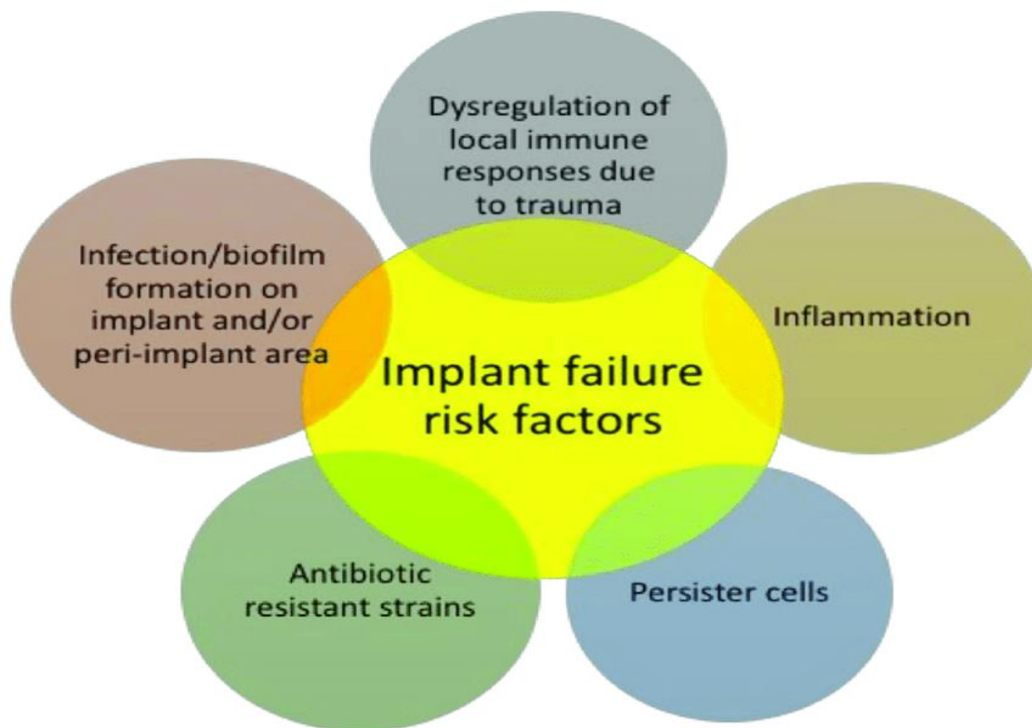
Figure 1.5: Medical implant failure risk factors [72]

1.8.2 Significance of Hydroxyapatite (HA) coating loss

The HA coating is retained on the surface of the substrate. Duchene noted that the coating function cannot be maintained for the life of the patient. He suggested that it should be absorbed to regrow bone and also to stabilize the implant. Bone growth on the implant surface is a balance between the release of calcium and phosphate ions and bone formation. The loss resulting from removing the coating may be on the surface of the implant. Widespread is a serious coating quality problem and may result in implant loosening [73].

1.9 Thermal Spraying

Thermal spray uses high temperature and speed to melt the powder and is divided into two categories: chemical energy, the combustion gases that operate the flame spray, and electric currents [74]. Various different techniques are currently available for deposition of calcium phosphate (CaP), in particular hydroxyapatite (HA) coating, to metallic materials, including plasma spraying , magnetron spraying (RF), sol-gel method, flame spraying...etc. [75]:

1.9.1 Radio Frequency- Magnetron Sputter (RF - Magnetron sputter)

The RF-Magnetron spray allows controlling the properties of CaP films within a fairly wide range and forming a dense and uniform coating for devices with complex formations with high adhesion and uniformity in thickness and composition. It is a rather complex method, especially for the deposition of multicomponent materials such as calcium phosphate. There are many process parameters that can have a direct effect on the properties of the coating. For example, the coating composition can be affected by spray parameters such as gas pressure, substrate bias, and deposition temperature. During the RF-Magnetron spray, the dense plasma interacts strongly with the substrate [76],

which causes intense ion bombardment of the coating. During RF discharge, positive ions are accelerated and bombardment of the substrate with high energies, the properties of RF-Magnetron sputter film are strongly affected by bombardment of the film with types of discontinuous target and from plasma. The latter is determined by deposition parameters such as working gas pressure and composition, target substrate distance, and substrate bias voltage. Different energy and temperature conditions may result in a different final quality and structure of the applied coating. Control of these parameters is essential to modify the structural properties, composition and mechanical properties of the HA coating.

1.9.2 Plasma spraying

Among the listed methods, plasma spraying is the only commercially approved method for depositing HA layers on metallic implants. The method is based on the formation of an intense layer of particles deposited on a metal substrate. The particles that originate from the powder material are conveyed by a gaseous stream and pass through an electric plasma generated by a low-voltage and high-current electrical discharge. During this process, hot particles crystallize and agglomerate during film formation. Coating features are determined by the chemical and mechanical properties of the powder material used, the distance between the source and the substrate, the electric arc current, the deposition rate and the composition of the working gas. Plasma spraying allows the production of coatings up to 300 μm in thickness. This technique has some important limitations: poor uniformity in coating thickness and substrate adhesion, low crystallinity, poor mechanical properties on tensile strength, wear resistance, hardness, and fatigue [77]. While the main drawback of this method is that a higher temperature (6000-10000°C) is used during

plasma spraying, the crystal structure of HA powder can easily be destabilized and decomposed into a mixture of HA, CaO, tri-calcium phosphate, tetra-calcium phosphate and a large amount of non-phase Crystallization occurs [78]. Structural heterogeneity can lead to differences in coating resorption and reduced substrate interfacial strength of the coating [79, 80].

1.9.3 Sol-gel deposition

Sol-gel deposition is a common method for producing Calcium phosphate (Cap) coating [81] this method is based on the preparation (a colloidal solution) with its subsequent transfer to a gel and treatment of the metal surface with the resulting colloid. This method makes it possible to produce a dense CaP coating with a thickness of 0.5-30 μm. Sol-gel deposition is a relatively inexpensive technique compared to the others. This method has the potential to intricately cover the implant using a simple setup [82]. Moreover, the main advantages of the sol gel method are good mechanical properties, abrasion resistance, and adhesion strength due to its nanostructure [83, 84]. However, sol gel deposition has drawbacks such as high permeability, low wear resistance, and difficult porosity control, which hampers its commercial application [85].

Table 1.1 the advantages and disadvantages of the most applied methods for HA coating deposition. [86]

Technique	Advantages	Disadvantages
RF-magnetron sputtering	dense, pore-free coating; ability to coat heat-sensitive substrates; High purity films able to control coating structure and Ca/P ratio; Good adhesion (30 MPa)	low deposition rate; expensive
Plasma spraying	High deposition rate Low cost The coating usually has a delicate surface and porosity	poor adhesion, poor mechanical properties, wear resistance, hardness, high

		temperatures lead to structural heterogeneity; Rapid cooling results in cracks in the paint
Sol-gel coating	Inexpensive, high purity; fairly good adhesion (40 MPa); It can cover complex substrates.	high temperatures; High permeability, low wear resistance; Difficulty controlling porosity

1.9.4 Flame spray pyrolysis (FSP)

Flame spray pyrolysis is an economical and versatile process as in metals and alloys [87]. Flame spray pyrolysis is described as the process of cracking and delivering droplets to a high-temperature reactor where the solvent evaporates and the remaining solute reacts with the surrounding gases [88].

The flame-spray pyrolysis process is strong, and different flame formations are used to manufacture nanoparticles, such as pre-mixing and diffusion. The formation of flame spreads and the fuel and mixing are the combustible gases before they enter the flame area [89].

In spray pyrolysis, it leads to the decomposition of particles at a high temperature and produces a useful powder, as well as converting the material into drops and entering it in a hot place. The heat source causes the solute to evaporate in the drops, and the solute precipitates and decomposes, which results in excellent and homogeneous particles and is easy to use in applications [90].

Spray pyrolysis is a multi-use technology that has been applied to the synthesis of many oxides and metals due to its simplicity and ease. When using a flame in FSP, the material is exposed to a high temperature of more than 1000 ° C. The hot combustion products are used as a source of heat at which the product is produced [91].

The FSP method also provides great flexibility in terms of selection of precursors and flow controls, which in turn determine the amount of material produced. The particle formation can be described as a series of complexes whose particle size ranges from a few to several hundreds of nanometers, depending on the operating conditions. A typical FSP process consists of a central nozzle injecting a solution of a substance (usually containing the metal or metals of choice such as silicon, titanium, iron, etc.) and a solvent (for example, ethanol, acetonitrile, or xylene, etc.). The nozzle is surrounded by a fast-flowing dispersion gas (pure air or oxygen) this enhances the atomization of the liquid solution and provides the oxidizer needed for the combustion of the liquid mixture. Next to the dispersion gas, air or oxygen is introduced, helping to stabilize the spray flame. An external flame source, usually oxyhydrogen or ox hydrocarbon, is used, which is required to support the combustion. The droplets from the atomization near the nozzle are vaporized and ignited by the supporting guide flame resulting in a spray flame. Higher temperatures inside this flame lead to the formation of nanoparticles [92]. A variety of products can be manufactured with FSP, such as zinc oxide, titanium oxide, and zirconium oxide [93].

Several diagnostics in FSP, such as X-ray, transmission electron microscopy (TEM), moving particle size scanning (SMPS), particle mass spectrometry (PMS), can be used to characterize the associated particle diameter and distribution Other techniques are used to characterize spray droplets and flame spray .

1.9.4.1 Types of Flame spray pyrolysis (FSP)

Flame pyrolysis has been classified into three different types:

1- Flame-assisted pyrolysis (FAP): Metal particles are used that volatilize and are fed in the flame. The metal particles are converted into particles in the gas phase. This method has drawbacks. The products are limited in this method because they need volatile particles [94].

2- Flame-Spray Pyrolysis (FSP): It uses non-combustible mineral particles (aqueous solutions of mineral salts) and flames consisting of hydrocarbons [95].

3- liquid Flame-spray pyrolysis (LF-SP): The process uses metal oxide in the form of metal chlorides and is characterized by short time and homogeneous nano-sized particles [96].

1.10 Structural properties:

Structural characteristics are important for the study structure of thin films and are done using X-ray diffraction.

1.10.1 X-Ray Diffraction (XRD)

X-ray diffraction technique is a powerful tool for material characterization. This technique is applied not only for structure determination of solids but also to some other problems, such as chemical analysis, stress measurement, study of phase equilibrium, determination of particle size, determination of orientation of crystal. We know that the physical properties of solids (e.g. electrical, optical, magnetic etc) depend on atomic arrangements of materials, so the determination of the crystal structure is an indispensable part of the characterization of materials. Indispensable part of the characterization of materials. X-rays are used to establish the atomic arrangement or structure of the materials because the interplanar spacing (d_{hkl}) of the diffracting planes

is of the order of X-ray wavelength. For a crystal with a given d-spacing and for a given wavelength λ, the various orders n of reflection occur only at the precise values of angle θ, which satisfy the Bragg equation [97]:

$$n\lambda = 2d_{hkl}\,sin\theta$$ …………… (1.1)

   As shown in Figure (1.6), where d is the spacing between the planes, θ is the angle that the X-ray beam makes with respect to the plane, λ is the wavelength of the X rays, and n = 1,2,3, . . . is an integer that usually has the value n = 1. The distance d between parallel crystallographic planes with indices (hkl) for a simple cubic lattice of lattice constant as the particularly simple form [98]:

$$d = \frac{a}{(h^2+k^2+l^2)^{1/2}}$$ ……………… (1.2)

To estimate the average crystallite size of nanoparticles from the   measured width of their diffraction curves (XRD pattern), we used the Scherer formula [98]:

$$D = K\lambda\,/\beta cos\theta \ldots \ldots \ldots \ldots \ldots \ldots \ldots \ldots \ldots \ldots (1.3)$$

In this equation, shape factor (K) =0.9, λ represents the wavelength of the X-ray radiation, β is the full width at half maximum of the diffraction

Peak (in radians) and θ is Bragg diffraction angle of the diffraction peak.
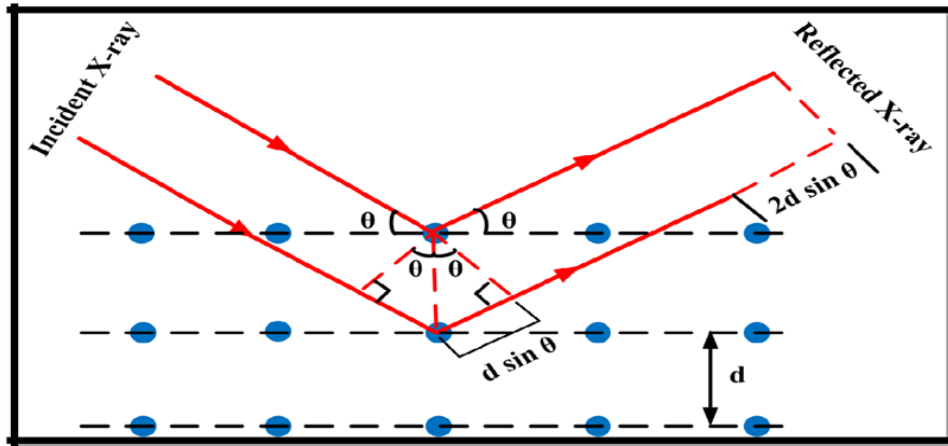
Figure 1.6: Determination of lattice spacing using Bragg's law [99]

1.10.2 Field Emission Scanning Electron Microscopy (FESEM)

Field Emission scanning electron microscopy (FESEM) is a powerful morphological technique, which allows observing the surface, topography and relief of a material from images using electrons. The working of a scanning electron microscope is based on the use of electrons rather than light to form an image of objects. The shorter wavelength of electrons permits image magnifications higher than conventional light microscopy. The detector equipment is very sensitive being able to reveal details up to 1-5 mm in size and thus must operate within an ultra-high vacuum for accurate measurement as Figure (1-7) [100].
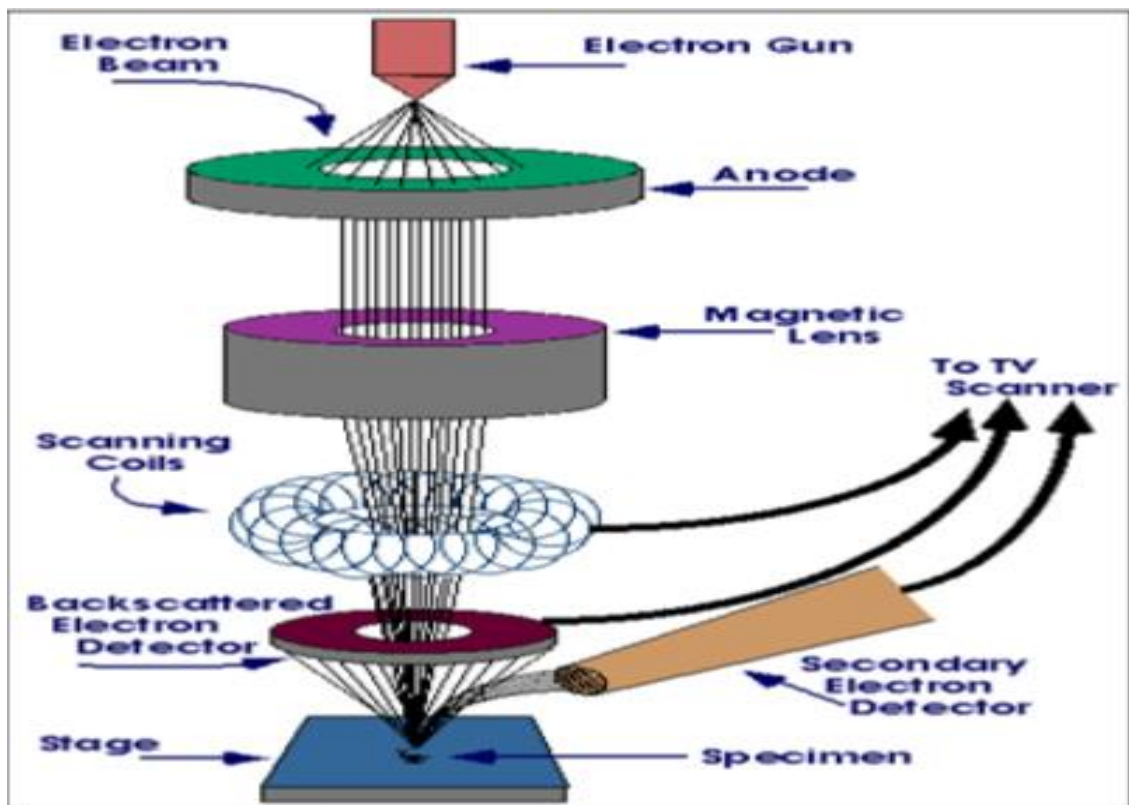
1.7: Block diagram of Field Emission Scanning Electron Microscope [100].

1.10.3 Fourier Transformed Infrared Spectroscopy (FTIR)

The FTIR spectroscopy is a powerful modern technique in which spectrum is first produced as an interferogram which is processed and computed in real time through a dedicated computer to provide high resolution information. Infrared spectroscopic studies are carried out. Infrared spectroscopy provides information about the concentration of the impurities, and their bonding with the host material. In FTIR, the infrared radiation is split into two beams, out of which one is kept static and the other moving. These are combined to give a modulated beam which is passed through the sample. It is then digitized and Fourier transformed by the computer to give the infrared spectrum.

FTIR spectroscopy has the following applications:

a) Useful spectral information can be obtained from a sample of a microgram or less. Utilizing special techniques, as little as 50 pictograms may be analyzed.

b) A spectrum can be obtained in much shorter time than is possible with a dispersive spectrometer.

c) The spectrum can be obtained at very high resolution, which has certain advantages in studying small molecules in vapor phase.

d) Give information about chemical bonds [101.102].

1.11 Methods of Evaluation of Antimicrobial Activity

Nowadays, various methods for assessing the antigenic activity are discussed, and their results are presented differently. The method and method of its dissemination and method of dissemination is the method of distribution, which was developed in 1940. The procedures are as follows:

1. Prepare agar plates incubated with a standard inoculum of microorganisms for testing.

2. Sterile discs (about 6 mm in diameter) are placed on the surface of the agar.

3. Place the cultured agar plates in an incubator under conditions suitable for the tested bacteria.

4. The sensitivity of the tested organisms is determined by measuring the diameter of the damping area around the disc or well. This method is considered advantageous for its simplicity and low cost and is commonly used for its antibacterial activity [103].

The antibacterial and antifungal activity of the particles is being studied against Gram-negative bacteria (K.pneumoniae, P. Aeruginosa) and (E. coli), and Gram-positive bacteria (S. aureus). And against a type of fungi (Candida albicans) by measuring the diameter of the inhibition zones for each sample.

1.11.1 Fungi

Fungi are any member of the kingdom of organisms that lack chlorophyll, true leaves, stems, and roots, reproduce by spores, and live as fungi or parasites. The group includes mold, mildew, and rust [104].

1.11.1.1 Candida Albicans

It is an incomplete yeast form classified within the kingdom of fungi most species of Candida are usually found in the environment, approximately a dozen or so are associated with colonization and infection of humans. Candida species are common in the oral cavity, intestinal tract, and vagina, and newborns are colonized soon after birth. While this species is harmless in most individuals, under certain conditions it can multiply opportunistically and cause a variety of diseases. These diseases range from superficial infections of the mucous membrane to life-threatening systemic infections that can spread through the bloodstream to all parts of the body. However, other Candida infections are largely attributable to host-related defects. Such as HIV infection [105]. Albicans is able to form a well-organized 3D biofilm containing yeast, hyphae, pseudo saccharides, and exopolysaccharides that prevent entry of antifungals and protect the organism from host immunity [106].

1.11.2 Bacteria

The term bacteria was coined by German scientist Ferdinand Kuhn in the 19th century, and is based on the Greek word "bacterium". They are unicellular

microorganisms devoid of chlorophyll, and reproduce by simple mitosis, often assembling in round, stick-like, spiral or nodule unicellular or acellular bodies [107].

They can be divided into two main categories based on differences in the structural composition of their cell wall. They are Gram-positive bacteria and Gram-negative bacteria. The names arose from the staining technique developed by Hans Christian Gram in which the two types of cell wall can be differentiated. Gram-positive bacteria have a thick cell wall and contain up to forty layers of peptidoglycan that color dark purple when exposed to the primary dye, crystal violet, while Gram-negative bacteria have only a few layers of peptidoglycan, which are pink because they retain the pigment an antihistamine called safranin in general, Gram-negative bacteria are more pathogenic than Gram-positive bacteria. This is due to several factors, including that the Gram-negative bacteria have an extra outer layer coated with hydrophilic lipopolysaccharides, which prevents many lipophilic antibiotics from entering the cell. In addition, many antagonists disrupt the mechanisms that form cross-links in the cell wall. Silver has been distinguished over traditional antibiotics in the fight against gram-negative bacteria such as Escherichia coli, as the hydrophilic nature of silver ions enables it to enter into gram-negative bacteria naturally effective through the pores of the outer membrane. However, entry into Gram-positive bacteria is also more difficult due to the presence of a hydrophobic peptidoglycan layer and the lack of membranous pores [108].

1.11.2.1 Klebsiella Pneumoniae (K. Pneumoniae)

It was first described in 1882, by Karl Friedlander. He described it as an encapsulated bacillus after isolating the bacteria from the lungs of those who

had died of pneumonia. Originally called Bacillus Friedlander, the bacterium acquired the name Klebsiella. Klebsiella pneumonia in 1886. They are Gram-negative, encapsulated, and non-motile bacteria. Bacteria commonly colonize human mucosal surfaces of the oropharynx and gastrointestinal tract [109], have recently gained notoriety as an infectious agent due to the high number of severe infections and the increasing paucity of effective treatments. Due to the emergence of strains of them that have acquired additional genetic traits and become either hypertrophic or resistant to antibiotics. It also has the ability to escape rather than suppress many components of the immune system and grow in many sites in the host and thus survive [110].

1.11.2.2 Staphylococcus Aureus (S. aureus)

Staphylococcus aureus is a spherical (Gram-positive) bacterium with a diameter of about 1μm. The division of its cells occurs in more than one plane, and grape-like clusters are formed. It is a dangerous human pathogen. It is a common infection of intact skin, skin glands, and mucous membranes, is found in about 30% of healthy humans and usually colonizes the nose and skin. Staphylococcus aureus can cause bloodstream infections, endocarditis, skin infections, soft tissue and joint pneumonia, and bone infections. Under certain conditions .Staphylococcus aureus can survive on complex nutrients such as amino acids and vitamins [111].

1.11.2.3 Escherichia coli (E. coli)

The are facultative anaerobic bacteria, first described by Theodor Escherichia in 1885. Most strains of E. coli harmlessly colonize the gut of humans and animals. However, there are some strains that have evolved into pathogenic E. coli usually Gram-negative, rod-shaped (2.0-6.0) μm in length

with rounded ends. However, the actual shape of these bacteria differs from spherical cells in that they are elongated rods or filamentous. It is also not a sporophyte, and usually moves by the action of a peritoneal flagella [112].

1.11.2.4 Pseudomonas aeruginosa (P. Aeruginosa)

Pseudomonas aeruginosa is a Gram-negative, rod-shaped bacterium with a length of (1.5-3) μm that can be described as an aerobic organism, except that it can live in an environment with little or no oxygen. They are often present in water and soil, transported by flagella or attached to surfaces as a biofilm. It can live in different physical conditions such as very high temperatures. It is considered one of the main causes of infection among hospitalized patients, and the reason is due to its clear tolerance to detergents, disinfectants and antimicrobial substances, as well as among people with weak or immunodeficiency. They usually cause bloodstream infections, urinary tract infections, and hospital-acquired pneumonia [113]. Cystic fibrosis or COPD [114].

1.12 Literature Survey

Many studies and research have been conducted and published, many of these studies are related to the current work, part of which will be presented:

Oyane and Ayako (2010) [115] developed a new biomimetic process for coating apatite on polymeric materials. In this process, the polymer surface is modified with calcium phosphate and then the polymer is immersed in a supersaturated calcium phosphate solution. The new biomimetic process has advantages of safety, simplicity, and applicability to various types and shapes of polymeric materials. By adding a biomolecule (such as a protein, antibacterial agent, or DNA) to the solution, the biomolecule can be fixed in

the apatite coating while retaining the intrinsic biological activity of the biomolecule. As a result, the base polymer has biological activity, as well as good biocompatibility due to apatite. Hence, the novel biomimetic process and the resulting compounds have a variety of biomedical applications including gene delivery vectors.

Chavan *et al.***, (2010) [116]** noted Hydroxyapatite (HAp) is the main mineral component of magnetic tissue. It is widely used in bioactive, bioactive and biocompatible biomedical applications. HAp nanoparticles are synthesized by wet chemical dosing fabricated with XRD, FTIR, AFM and SEM for structural and morphological formulations and group analysis. Mimic body fluid (SBF) is prepared using chlorides, carbonates, oxides, and metal sulfates at 37 °C. XRD concentration analysis of the hexagonal phase of hydroxyapatite. FTIR appears Existence of groups and functions. SEM observations reveal that the growth of a highly porous apatite layer and Surface increases over time.

Waterman *et al.***, (2011) [117]** used calcium phosphate bio-coating on magnesium substrates via a biomimetic coating process. The effect of pretreatment of magnesium hydroxide on the formation and maximum corrosion protection of coatings was studied. The corrosion resistance of the coating was studied in the laboratory using a simulated body fluid, where it was noted that the corrosion resistance increased in the solution due to the additional calcium phosphate from the liquid to the substrate.

Oyane *et al.***, (2012) [118]** aimed to use layers of calcium phosphate compound and the use of bioceramic materials, which are conductive to the bones, and are used in medical applications in dental implants and dentistry,

where calcium phosphate particles are biocompatible and biologically active. Calcium phosphate was applied to the surfaces of the base materials by a biomimetic process using solutions. Thus they provide a biocompatible surface and these layers have been characterized in in vivo tissue regeneration and biological transport, and these composite layers, due to their good biocompatibility and controllability of cell behavior on their surfaces, have great potential in tissue engineering applications.

Surmeneva *et al.*, **(2013) [119]** prepared a thin biocompatible hydroxyapatite coating on substrates such as silicon and titanium. Energy-dispersive X-ray spectroscopy (EDX) gave Ca/P molar ratios of 1.78, respectively. According to the XRD analysis, the nanocrystal coating had a crystal size in the range of 10-50 nm. The coating substructure was analyzed by high-resolution transmission electron spectroscopy (HRTEM) combined with fast Fourier transform (FFT) analysis. The average crystal size calculated was in good agreement with the HRTEM results. The immersion of the coated substrates in simulated body fluid (SBF) resulted in the deposition of the apatite layer.

Amaravathy *et al.*, **(2014) [120]** used Magnesium alloys which are a new class of biodegradable alloys that have many preferred properties to overcome the limitations of currently used biomedical alloys. Several coatings have been developed to overcome the high rate of decomposition. In this regard, a new attempt has been made to develop a Hydroxyapatite Hydroxyapatite/TiO2 coating on magnesium alloys to increase biocompatibility and reduce corrosion rate. The coated surfaces were characterized by Fourier transform infrared spectroscopy (FT-IR), X-ray diffraction (XRD), scanning electron microscopy (SEM) using energy dispersive X-ray spectroscopy (EDX), atomic force

microscopy (AFM) and electron microscopy. Transmission (TEM)   in vitro studies showed that the HA-TiO2-coated alloy exhibited higher osteogenic catalysis compared to the HA-coated alloy.

Rojaee *et al.*, **(2014) [121]** used Coating of fluorinated hydroxyapatite nanopowders with different degrees of fluorescence on microarc oxidized magnesium alloy AZ91 via electrophoretic deposition method. Conductivity techniques have been used to provide suitable conditions for the coating. The bio-corrosion process and associated mineralization during immersion in a liquid body solution have been explained. Based on the results, a 25% fluorine-substituted hydroxyapatite coating on the microarc-treated AZ91 implant has been suggested to aid bone growth and without postoperative complications during its lifetime.

Dorozhkin *et al.*, **(2015) [122]** used different types of materials to replace damaged bones, including porcelain, which is a potential bone graft due to its biomechanical properties. A little later, these synthetic biomaterials were called bioceramics. Bio ceramics can be prepared from calcium phosphate (CaPO4) only, which possesses definite advantages due to its chemical similarity with bone. Current biomedical applications of CaPO4-based bioceramics include bone augmentation processes, bone grafts, and bone grafts. Prosthetics, maxillofacial reconstruction, spinal fusion, periodontal disease repair, orthopedic filling after oncological surgery. CaPO4 appears to be a promising carrier of growth factors and is biologically active.

Kattimani *et al.*, **(2016) [123]** noted hydroxyapatite (HA) is an essential component required for bone regeneration. Various forms of HA have been used for a long time. HA is famous for bone regeneration through conduction

or through action to fill defects from antiquity, but emerging trends of bone inductive property of HA is very promising for new bone regeneration. Calcium apatite nanostructured plays an important role in building tissues. Use biocompatible materials from nanostructured bioceramic particles of importance in artificial bone grafts and bone cement, so that these compounds enhance the strength of the bioceramic.

Teo *et al.***, (2016) [124]** made use of polymers as biomaterials due to their ease of fabrication, flexibility, and biocompatible nature as well as a wide range of mechanical, electrical, chemical and thermal behaviors when combined with different materials as composites. Polymeric materials also have great tensile strength and must be able to hold the device over the life expectancy of the implant.

Shin *et al.***, (2017) [125]** developed synthetic biomaterials impregnated with the organic and inorganic properties of natural bone Calcium phosphate (Cap) has been mostly used to mimic the inorganic components of bone, such as calcium hydroxyapatite, due to its intrinsic bioactivity and bone conductivity and to enhance bone conductivity through incorporation of bone biomolecules. In this study, note the advantages and current advances of biomimetic surface mineralization processes using simulated body fluids for coating bone-like carbon apatite on the surfaces of various materials such as metals, ceramics, and polymers. The osteoinductive effects of incorporating biomolecules such as proteins, growth factors and genes into metallic coatings are also discussed.

Jodhani *et al.***, (2017) [126]** noted that functional metal oxides can exist in many different forms. Use the flame spray pyrolysis (FSP) method. This is a

fast and scalable hardening process that can be used for Nano powder synthesis.

Solero *et al.*, (2017) [127] flame spray pyrolysis method to produce different particles. The device consists of gas-assisted spraying to generate droplets and disperse in a secondary pilot flame. By dissolving suitable materials in liquid fuels, different types of nanoparticles were produced. Such as fabricating SiO2 and TiO2 and characterizing them by TEM and XRD analysis, respectively, and studying the operating conditions (eg, concentration of materials used) for the experimental device. Where we note the stability and reproducibility of the reaction flame, and thus the materials produced and the results obtained.

Rukosuyev *et al.*, (2018) [128] aimed to use flame spray pyrolysis, which is widely used in the chemical industry, which is a nanoparticle manufacturing technique. The spray pyrolysis method uses aqueous solutions. Where process parameters such as concentration and size of droplets and the ratio of air and gas mixture affect the size of nanoparticles, the solution is formed of silver nitrate (AgNO3) and it was found that silver nanoparticles were precipitated with an average size of 25 ~ 115 nm.

Neto *et al.*, (2018) [129] explained flame spray pyrolysis (FSP) is a well-known process for nanoparticle production and offers several advantages when compared to others, especially in terms of final product purity and operational flexibility. Considering that temperature and chemical composition throughout the reactor are essential for nanoparticle development in this work, zirconia (ZrO2) nanoparticles were produced via FSP and the combustion of the precursor solvent mixture was described through seven sets of different

chemical reaction mechanisms to analyze their effect on flame temperature and evolution particles during operation. The temperatures and diameters of the elementary particles obtained from the simulations are within 9% and 6% accuracy of the experimental values, respectively. Although there were mismatched temperature profiles for the different mechanisms considered (mainly in the lower regions of the reactor), a small variation in the diameter of the primary particles was observed when comparing the cases.

Furko *et al.*, **(2019) [130]** interested in the development of biologically active calcium phosphate layers Coatings were deposited on titanium alloys containing sufficient amounts of calcium nitrate and dihydrogen ammonium phosphate at 70°C. Energy-dispersive X-ray spectroscopy (EDX) as well as XRD and FT-IR measurements. The results revealed a CaP layer that is mainly in the hydroxyapatite phase. The coatings were evaluated in conventional simulated body fluid (SBF) over a period of 2 weeks. Electrochemical results showed that the pure calcium phosphate (CaP) coated implant material and implant have the highest corrosion resistance and biocompatibility.

Ji *et al.*, **(2019) [131]** noted that titanium (Ti) and its alloys are among the best materials for bone repair and replacement. However, as Ti-based minerals have low surface bioactivity and low bond strength with bone tissue, surface modification of Ti-based implants is important for improving surface bioactivity and biocompatibility. In this study, we prepared a ceramic coating containing calcium (Ca) and phosphorous (P) on Ti characterizing the coating by electron microscopy, energy dispersive X-ray spectroscopy, and atomic force microscopy to study the surface morphology, calcium and phosphorous contents, and surface terrain. A nanoscale distance test was performed to

determine the exact modulus of elasticity and fine stiffness. Which has shown good bioactivity, mechanical performance and has applicability.

Wang *et al.***, (2020) [132]** used strontium (Sr) and magnesium (Mg) to promote osteoblast proliferation and accelerate bone formation. However, the bio functional effect on Osseo integration caused by coating dental implants with hydroxyapatite (HA) comprising these two components of this study was to examine bone formation and Osseo integration in HA-coated titanium. Osseo integration of implants the results showed that among the groups tested, Outgrowths are found on new bone growth prominent bone and bone tissue suffering In addition, the greatest contact between bone and implants was found This study is the first of its kind to indicate flame-sprayed HA Sr- and Mg-doped coatings on titanium surfaces act on Osteogenesis therefore, suffer from low bone density.

Capellato *et al.***, (2020) [133]** suggested that the development of biomaterials and their potential use in medical cultures, where titanium was used as a suitable choice in implants and medical devices, and the recent results were surfaces of materials that offer bio morphology that provides nan architectures that have been shown to offer bio-functional and topographical surface modifications with a positive effect between the response of the material and the host.

Rezaei *et al.***, (2020) [134]** used various methods of surface modification of orthopedic and dental implants such as deposition of biocompatible coatings on implant medical surfaces. In this study, hydroxyapatite/hydroxyapatite-Mg double layer coatings applied to 316 LVM stainless steel were examined. The applied coatings consist of a dense layer of plasma sprayed hydroxyapatite and

a top layer of a magnesium hydroxyapatite composite coating. The coated samples were characterized by X-ray diffraction (XRD), scanning electron microscopy (SEM) and Fourier transform infrared spectroscopy tests (FTIR). The coated samples were evaluated by immersion of the samples in simulated body fluid (SBF) followed by plasma spectroscopy. Microscopic studies of the coated samples after corrosion tests showed that the magnesium component of the upper layer was degraded in the dissolved SBF. The results of the spectroscopy analysis showed that the double-layer coating systems prevent the release of toxic elements in the substrate such as nickel. The results of SBF immersion tests showed that the double-layer coating system improves the biocompatibility and bioactivity of 316 LVM stainless steel.

Naderi *et al.*, **(2021) [135]** noted that hydroxyapatite (HA) coated metal coatings are biocompatible compounds, which have potential for various applications for bone replacement and regeneration in the human body. In this study, we proposed the design of flexible and biocompatible composite implants using metal mesh as a substrate and HA coating as a bone regeneration activator derived from the simple sol-gel method. Experiments were performed to understand the effect of coating method (dip coating and drop casting), Substrate materials (titanium, stainless steel) and substrate mesh properties (mesh size, weaving pattern) on implant performance. Samples coated with HA were characterized by an X-ray diffractometer, transmission electron microscope, field emission scanning electron microscope, Nano center, polarization and biocompatibility assay. A pure or two-phase HA coating was obtained on substrates of different thicknesses. The results indicated that first-grade HA-coated titanium had the best performance as a

potential implant, HA-coated 316 stainless steel constituted a convenient and low-cost alternative.

Shunmugasundaram *et al.*, (2021) [136] used spray pyrolysis of three materials, tin oxide, copper, aluminum and steel, was used as substrate. The thin film was developed by spray pyrolysis with temperatures of 300°C for aluminum and 400°C for copper and steel, at a distance of 0.4m, where the result was that the strength increases by adding paint on the surface.

Liu *et al.*, (2021)[137] interested in the success of medical and biological implants in orthopedic and dental applications where titanium particles have been used that are related to bioactivity, we first focused on surface coatings to enhance the bone fusion and biocompatibility of implants by emphasizing the nanoscale scale associated with calcium phosphate. Various coating strategies such as plasma spraying, and simulation deposition were discussed bio, and then discussed anti-adhesion and bactericidal surface construction techniques with emphasis on multifunctional surface coating techniques that combine potential osseointegration and antibacterial activities. The result was the development of multifunctional surface coatings that combine osteogenesis and antimicrobial activity. Multiscale hierarchical surface structures with better biofunctional results were obtained.

Madero *et al.*, (2021) [138] showed flame spray pyrolysis (FSP) is a robust and scalable method for the synthesis of powders. However, there are many materials that cannot be synthesized by FSP because their properties degrade when exposed to high temperatures, a low-temperature flame pyrolysis process (LT-FSP) has been proposed, and the method is applied to the synthesis of lithium and manganese including Proposed LT-FSP process on

ethanol, added to an aqueous applicator, as a fuel. Unique in ethanol including high vapor pressure boosted by high activity coefficient in water - allows for stable combustion and low temperature after flame. Using a circular burner, a constant flame for the mixture was achieved, and the subsequent reactor temperature was found to be much lower than it could be obtained by conventional FSP. Controlled by changing the ethanol concentration, the physical properties of the manufactured materials were determined. It was also found that LT-FSP leads to improved material homogeneity when compared to other spray pyrolysis method.

Dasgupta *et al.*, **(2022) [139]** noted flame spray pyrolysis (FSP) is a method for large-scale production of nanoparticles and Nano powders in a wide range of industrial applications. A model of the FSP reactor was developed to simulate the coupling of the main phenomena involved in the particle synthesis process: liquid-spray dissociation and evaporation, mixing, combustion, and formation/growth of silica nanoparticles. Particle sizes and their distributions are validated against experimental data. Then, simulations are used to investigate the influence of process parameters on the resulting flame dynamics and particle growth. Showed that particle sizes are closely related to the precursor concentration in the solvent. At higher concentrations the diffusion is higher where the collision probability between particles is higher, the increase in the flow rate increases the length of the flame effect and finally it was found that the dispersion of the gas flow rate strongly affects the shape of the spray flame.

1.13 Aim of the work

1. Preparing biocompatible layer for medical implants using flame coating technique on metal substrates.

2. Characterization of the prepared samples at different parameters, the biocompatibility, and antibacterial activity for the prepared samples.

3. This study gives a picture of the possibility of accelerating the healing process and building the damaged bones.

C H A P T E R   T W O
EXPERIMENTAL WORK AND PROCEDURE

2.1 Introduction

This chapter describes the experimental work of this research, which includes a brief description of preparing the Calcium phosphate $Ca_3(Po_4)_2$ (Cap) films by the method of flame coating technique, coating samples of stainless steel and testing the possibility of using them in medical implants with layers compatible with human body.

The experimental part consists of the following steps:

1- Design and construction of a simple flame coating system

2- Cutting and cleaning stainless steel substrates

2- The films are deposited by flame coating method

3- Controlling the properties of deposited films by means of several factors (such as the distance between the flame and the base, the concentrations of the film material, and the ratio of the components)

4- The deposited films are examined by several techniques such as XRD, FESEM, FTIR, EDX, and Antibacterial effect

5- The deposited layers are tested by immersing the samples in a simulated body fluid to monitor the growth of layers biological activity of (calcium phosphate) on the deposited films.

6- Studying the antibacterial activity of the prepared layers against bacteria

Figure (2-1) shows the block diagram of the experimental work.

Experimental work and procedure

↓

Design and construction

Of a simple flame coating system

↓

Cutting and cleaning Stainless steel substrata

↓

Deposition of films by flame coating method

↓

Controlling the properties of deposited films by means of several variables

↓

The distance between the flame and the base

Concentrations of films substance

The proportions of the components

Measurements

Structural properties

Anti-Bacterial

XRD   **FTIR**   **FESEM**

Test the precipitated layers by immersing the samples in SBF

↓

XRD

Figure 2.1: Block diagram of the experimental work.

2.2 Substrate Preparation

The nature of the substrate is very important because it greatly influences the properties of the films deposited on it. The stainless steel type 316) is cut to the length of the piece of steel (2) cm in width and (1.5) smooth it out and it is ready. Then the substrates are cleaned because the effectiveness of cleaning the substrates has a strong impact on the adhesion properties of the deposited films as shown in Figure (2.2).

Figure 2.2: Stainless steel substrates preparation

2.3 Substrate (stainless steel) cleaning:

Substrate cleaning is critical to the success of the final applications of the material to achieve a contamination-free surface. Stainless steel slide substrates that are cleaned by:

1. The slides are cleaned with a soap solution to remove oily substances from the surface and then washed with water

2. The slides were placed in a clean beaker with distilled water and then immersed in an ultrasonic bath for 15 minutes.

3. It was repeated by replacing the distilled water with an ethanol solution to prevent contamination such as some oxides.

4. Air blow dries the slides and keeps them for use.
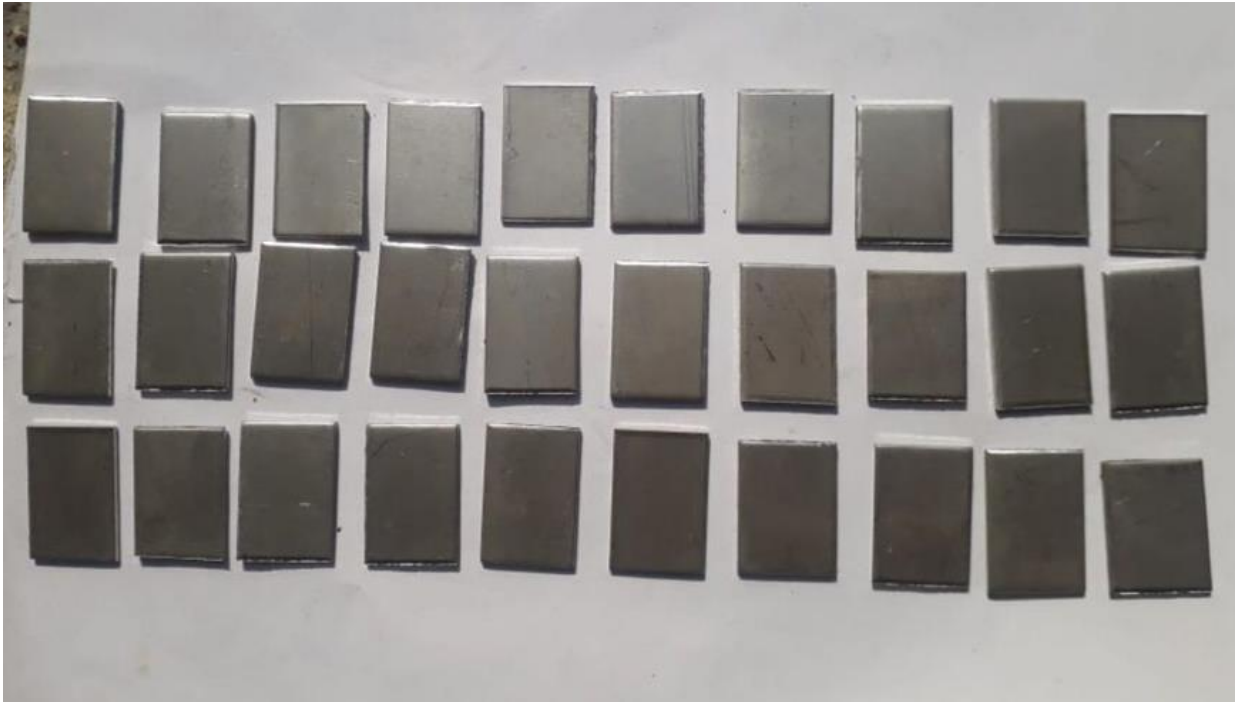
2.4 Materials

Calcium nitrate (Ca $(NO_3)_2$:$4H_2O$) of 98% purity, di-ammonium hydrogen phosphate $(NH_4)_2HPO_4$> 99% purity (Merck Co.), and Ammonium hydroxide solution (NH_4OH) from Alpha Aesar (Chemical Co.) are used in this work.

2.4 Setup of construction system

In this research, a simple flame coating system was designed and built. The system consists of simple and locally existence parts, containing an air-compressor adjusted at a constant pressure of 4 bar and a nozel to spray the droplets of calcium phosphate in a very small size, as well as a small gas tube with a igniter. The substrates were installed using a holder in front of the flame at different distances (2, 3, 4, 5 and 6 cm) the liquid is sprayed inside a vertical tube passing only the very small drops enter the flame, interact with it and deposited on the substrates as shown in Figure (2.3) and Figure (2.4).
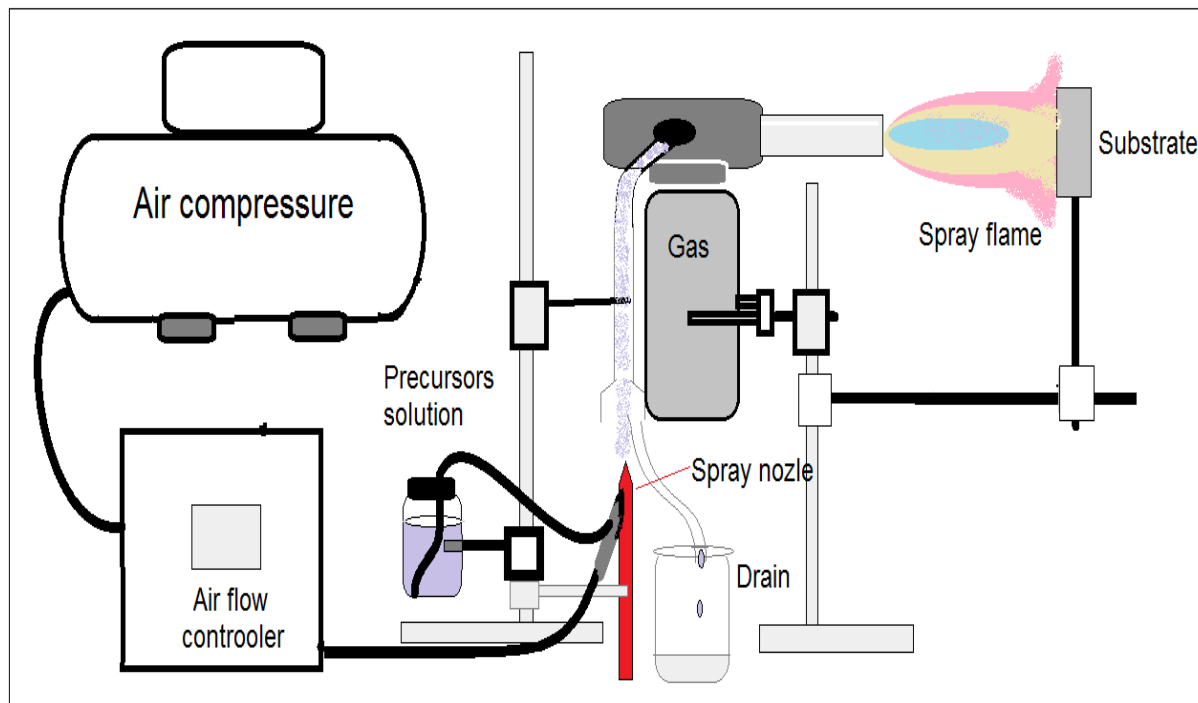
Figure 2.3: Flame coating setup

Figure 2.4: Laboratory image of the system

2.5 Preparation method of thin film

Stainless steel 316 substrates were cut and cleaned with water and then with ethanol. The calcium and phosphate solutions of 0.2 M prepared separately, and mixed at different Ca/P molar ratios (1.4, 1.5, 1.65, 1.8, and 1.9) then sprayed by nozzle throw flame using a pressure of 4 bar by control valve. The droplets interact with the flame and deposited on the stainless steel substrates at 3 cm from the flame orifice. Samples were prepared at different Ca/P ratios and deposited distances from the flame orifice (2, 3, 4, 5, and 6 cm) as shown in Table (2.1) and Table (2.2).

Table 2.1: The symbols of the samples of different Ca/P ratios

Symbol	Molar Ratio (x)			Weight in 50 ml D.W (g)	
	Ca/P	$Ca(NO_3)_2{:}4H_2O$	$(NH_4)_2HPO_4$	$Ca(NO_3)_2{:}4H_2O$	$(NH_4)_2HPO_4$
A3	1.4	0.5833	0.4167	1.3773	0.5503
B3	1.5	0.6000	0.4000	1.4166	0.5282
C3	1.65	0.6226	0.3774	1.4701	0.4983
D3	1.8	0.6429	0.3571	1.5178	0.4716
E3	1.9	0.6552	0.3448	1.5469	0.4554

Table 2.2: The symbols of the samples of different distances from flame orifice

Symbol	Distance from flame orifice (cm)
C2	2
C3	3
C4	4
C5	5
C6	6

Deposited distances from the flame orifice (2, 3, 4, 5, and 6 cm) we notice the best Deposited of the film at a distance of 3 cm, and at a distance of 2 cm no film is formed as shown in Figure (2.5).
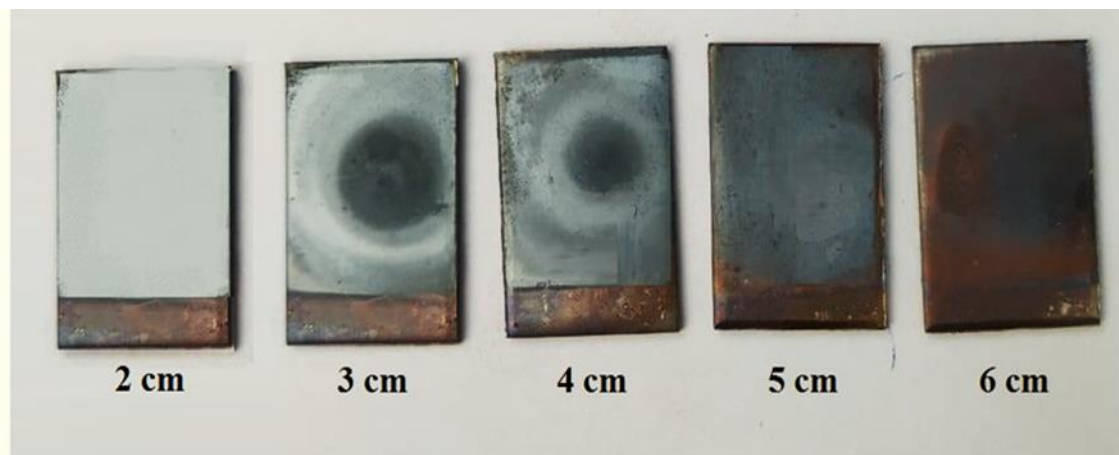
Figure 2.5: Stainless steel samples in different distances

2.6 Characterization Measurements

The biocompatible layers prepared on a stainless steel substrate at different ratios were characterized using different technique includes structural properties using x-ray diffraction (XRD) , surface morphology using the Field emission-scanning electron microscopy (FE-SEM), molecular structure using Fourier-transform infrared spectroscopy (FTIR).

2.6.1 X-ray Diffraction (XRD)

The structural properties for biocompatible layers prepared on a stainless steel prepared at different parameters were examined by XRD instrument (Shimadzu XRD 6000) with X-ray tube of Cu (K_α) radiation has monochromatic wavelength of 1.5406 Å, using 40 kV voltage high power supply and 30.0 mA current. The scanning angle was varied in the range of (2θ =20-80 degree) with speed 5.00 (degree /min).

2.6.2 Field Emission-Scanning Electron Microscopy (FE-SEM)

Field Emission-Scanning Electron Microscope model (MIRA3 TE-SCAN), is used to determine the surface morphology and elemental composition of the deposited layers by flame coating.

2.6.3 Energy Dispersive X-Ray Spectroscopy (EDX)

Elements contents are analyzed by energy dispersive x-ray spectroscopy (EDX). In electron microscope, electrons are used instead of light in optical microscope, because the wave accompanying the electron is very small comparing with light wave. The electron is accelerated and focused by electromagnetic lenses. X-rays emitted with different energies according to the characteristics electronic transition of elements.

2.6.4 Fourier-transform infrared spectroscopy (FTIR)

The chemical band were examined by FTIR using (Thermo Scientific Nicolet N10 FTIR Spectrometer)

2.7 Simulated Body Fluid Examination (SBF)

Simulated body fluid (SBF) technique was used to examine the biocompatibility of the deposited layers. The SBF was composed from the components shown in Table (2.3) [62]. The pH of SBF liquid is adjusted at 7.4 and 36.5°C temperature and noticed during the immersion period of 21 days to observe the growth of the hydroxyapatite layer on the substrates. The sample was re-examined by the XRD to determine the change in the sample structure of the film due to the deposited HAp layer on it.

Table 2.3: SBF components [62]

Reagents	g/L
NaCl	8.03
$NaHCO_3$	0.35
KCl	0.22
$K_2HP_4.3H_2O$	0.23
$MgCl_2.6H_2O$	0.31
$CaCl_2$	0.29
Na_2SO_4	0.07

2.8 Antibacterial activity

Diffusion disk antibacterial assay was used to examine the antibacterial of the deposited layer on Stainless steel (SS) substrate. The test was done by putting the calcium phosphate samples deposited on SS substrates at different Ca/P ratios of 5×5 mm$_2$ sample dimension over the agar surface spread with E.coli bacteria and incubated for 24 hours at 37 ℃. The inhibition zone was determine using special ruler.

C H A P T E R   T H R E E
## RESULTS AND DISCUSSION

3.1 Introduction

This chapter includes the results and discussions of this thesis. It is contains the results and analysis of experimental measurements in diagnostics of the prepared calcium phosphate layers on stainless steel substrates at different Ca/P ratios and different distances from the orifice of the flame sprayer. The diagnosis techniques include x-ray diffraction (XRD), field emission scanning electron microscopy (FE-SEM), Fourier-transform infrared spectroscopy (FTIR). Then investing the antibacterial activity of the prepared samples against two types of pathogenic bacteria are Gram-negative and Gram-positive bacteria. Finally, the biocompatibility of the deposited layers was examined, using a simulating body fluid, for use as medical implants.

3.2 Structural properties

The X-ray diffraction (XRD) patterns for the deposited layers at different Ca/P ratios (1.4, 1.5, 1.65, 1.8, and 1.9) using flame coating for substrate at 3 cm from the flame orifice were shown in Figure 3.1. All samples showed polycrystalline tetragonal structure of calcium diphosphate –beta phase matched with standard card (No. 96-100-1557)[140]. Many peaks appeared corresponding to the lattice planes (114), (211), (124), (215), (029), (02 11), (309), (263), (11 14), and (30 12) at diffraction angles 2θ= 24.2633°, 30.2369°, 33.2718°, 35.5600°, 43.1473°, 49.4099°, 53.5046°, 54.1068°, 57.0213°, and 62.5853°. Additional peaks for the stainless steel substrate appeared in all samples. Small variations in the peaks positions due to lattice strain as a result of variation in crystalline size or due to lattice defects [140]. The preferred orientation was along (215) direction. It is also obvious that the peaks intensity increased for the 1.65 Ca/P ratio and decreased for more ratio. On the other hand, the

width of the peaks decrease for the same ratio indicate on the highest crystallinety and growth of crystallite size.
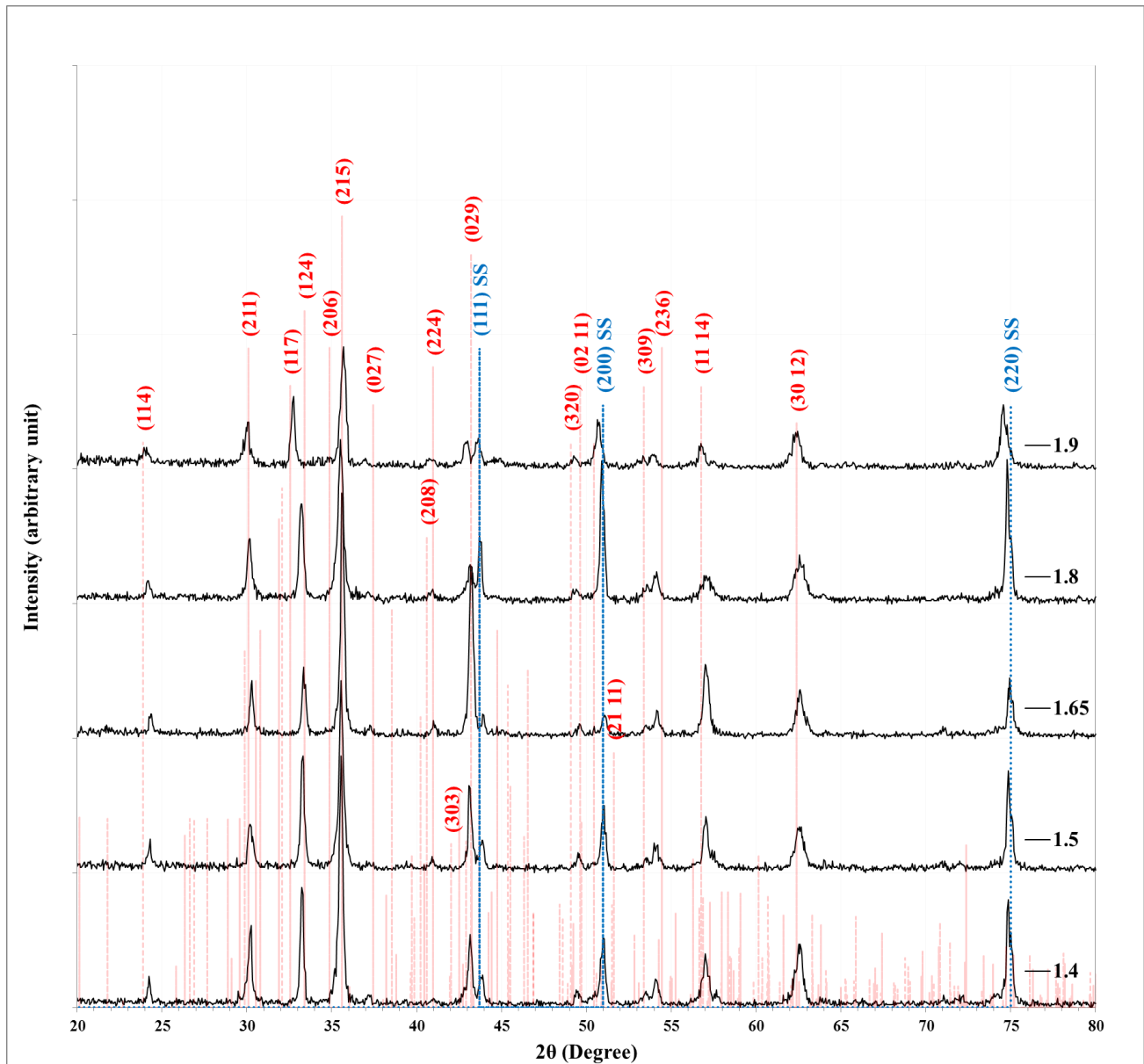
Figure 3.1: XRD patterns for calcium phosphate layers deposited at different Ca/P ratios.

Table 3.1 displays the diffraction angles, inter-planar distance (d_{hkl}) measured by Bragg's law, full width at half maxima (FWHM), crystalline size (C.S) measured by Sherrer's formula and the consistent Miller indices. Strain (ε) calculated by relationship
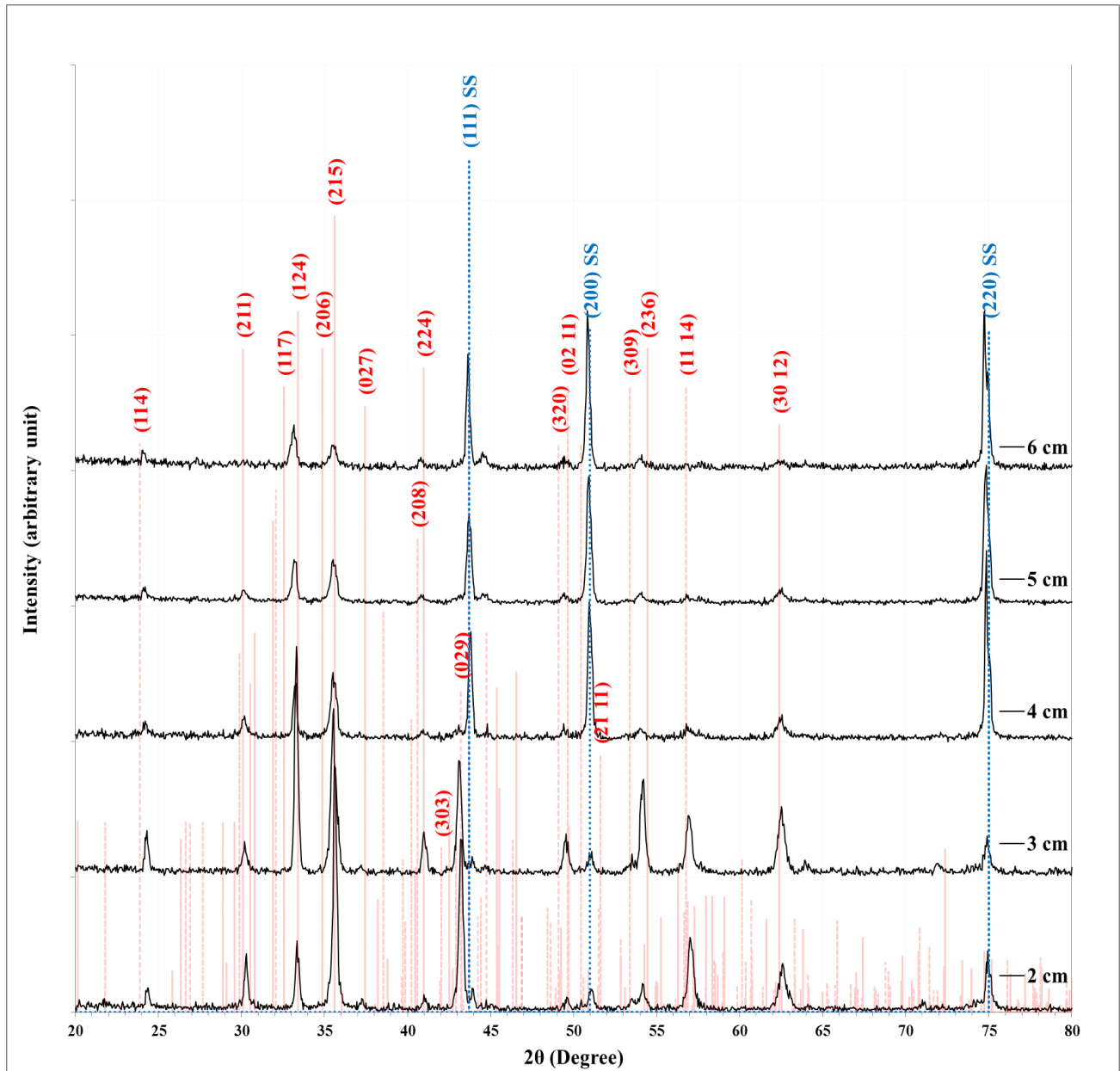
$$\varepsilon = \frac{\beta \cos\theta}{4}$$

The largest crystallite size appeared for the 1.65 Ca/P ratio.

Table 3.1: XRD parameters for calcium phosphate layers deposited at different Ca/P ratios.

Ca/P	2θ (Deg.)	FWHM (Deg.)	d_{hkl} (Å)	C.S (nm)	hkl	ε
1.4	24.2633	0.2650	3.6653	30.7	(114)	0.0011
	30.2369	0.2890	2.9534	28.5	(211)	0.0012
	33.2718	0.2890	2.6906	28.7	(124)	0.0012
	35.5600	0.3131	2.5226	26.6	(215)	0.0013
	43.1473	0.3131	2.0949	27.3	(029)	0.0013
	49.4099	0.3613	1.8431	24.2	(0211)	0.0014
	53.5046	0.3372	1.7113	26.4	(309)	0.0013
	54.1068	0.3372	1.6936	26.5	(236)	0.0013
	57.0213	0.5299	1.6138	17.1	(1114)	0.0020
	62.5853	0.5299	1.4830	17.5	(3012)	0.0020
1.5	24.2874	0.2409	3.6617	33.7	(114)	0.0010
	30.2128	0.3854	2.9557	21.4	(211)	0.0016
	33.2959	0.2891	2.6887	28.7	(124)	0.0012
	35.5600	0.2890	2.5226	28.9	(215)	0.0012
	43.1232	0.2650	2.0960	32.2	(029)	0.0011
	49.5303	0.3131	1.8389	27.9	(0211)	0.0012
	54.1068	0.3854	1.6936	23.1	(236)	0.0015
	57.0695	0.3372	1.6125	26.8	(1114)	0.0013
	62.5612	0.6022	1.4835	15.4	(3012)	0.0022
1.65	24.3838	0.2890	3.6475	28.1	(114)	0.0012
	30.3091	0.2890	2.9466	28.5	(211)	0.0012
	33.3681	0.3131	2.6831	26.5	(124)	0.0013
	35.6082	0.2650	2.5193	31.5	(215)	0.0011
	41.0277	0.3131	2.1981	27.1	(224)	0.0013
	43.2196	0.3131	2.0916	27.3	(029)	0.0013
	49.6026	0.3132	1.8364	27.9	(0211)	0.0012
	54.1790	0.4335	1.6915	20.6	(236)	0.0017
	57.0213	0.4335	1.6138	20.9	(1114)	0.0017
	62.5853	0.5299	1.4830	17.5	(3012)	0.0020
1.8	24.2152	0.3131	3.6725	26.0	(114)	0.0013
	30.1887	0.3613	2.9580	22.8	(211)	0.0015
	33.2477	0.3654	2.6925	22.9	(124)	0.0016
	35.5118	0.3854	2.5259	21.6	(215)	0.0016
	40.9314	0.2891	2.2031	29.3	(224)	0.0012
	43.1232	0.3613	2.0960	23.6	(029)	0.0015
	49.3617	0.3854	1.8447	22.7	(320)	0.0015
	54.1068	0.4336	1.6936	20.6	(236)	0.0017
	57.0695	0.5781	1.6125	15.6	(1114)	0.0022
	62.5853	0.7467	1.4830	12.5	(3012)	0.0028
1.9	24.0466	0.4576	3.6979	17.8	(114)	0.0020
	30.0682	0.3613	2.9696	22.8	(211)	0.0015
	32.7660	0.3131	2.7310	26.4	(117)	0.0013

35.7045	0.3813	2.5127	21.9	(215)	0.0015
42.9305	0.3853	2.1050	22.2	(029)	0.0016
49.2894	0.3854	1.8473	22.7	(320)	0.0015
53.9382	0.5058	1.6985	17.6	(236)	0.0020
56.7322	0.4577	1.6213	19.7	(1114)	0.0018
62.3444	0.5058	1.4882	18.4	(3012)	0.0019

The x-ray diffraction (XRD) patterns for the deposited layers for the selected ratio of 1.65 Ca/P using flame coating on stainless steel substrate at different distances from the flame orifice (2, 3, 4, 5, and 6 cm) were shown in Figure 3.2. Also the samples showed polycrystalline tetragonal structure. Nearly the same peaks observed with small shifts in the peaks positions due to lattice strain. The highest crystallinety appeared for the sample at 3 cm distance and decreased for more distances. on the other hand, the peaks corresponding to the substrates increased indicate on reducing the films thicknesses with increasing distance more than 3 cm. The preferred orientation converted from (215) direction at 2 cm to (124) direction with increasing the distance.

Figure 3.2: XRD patterns for calcium phosphate layers of 1.65 Ca/P ratio deposited at different distances from flame orifice.

Table 3.2 illustrates the XRD parameters for the calcium phosphate layers deposited at different distances. In general the crystallite size reduced with increasing the distance.

Table 3.2: XRD parameters for calcium phosphate layers deposited at different distances.

D (cm)	2θ (Deg.)	FWHM (Deg.)	d_{hkl} Exp.(Å)	C.S (nm)	hkl	ε
2	24.3089	0.2981	3.6586	27.3	(114)	0.0013
	30.2439	0.3523	2.9528	23.4	(211)	0.0015
	33.3062	0.2981	2.6879	27.8	(124)	0.0012
	35.5285	0.4336	2.5247	19.2	(215)	0.0018
	41.0298	0.3523	2.1980	24.1	(224)	0.0014
	43.1707	0.3523	2.0939	24.3	(029)	0.0014
	49.5664	0.3794	1.8376	23.1	(0211)	0.0015
	54.2005	0.3523	1.6909	25.3	(236)	0.0014
	56.9377	0.3794	1.6160	23.8	(1114)	0.0015
	62.5203	0.5149	1.4844	18.0	(3012)	0.0019
3	24.3838	0.2890	3.6475	28.1	(114)	0.0012
	30.3091	0.2890	2.9466	28.5	(211)	0.0012
	33.3681	0.3131	2.6831	26.5	(124)	0.0013
	35.6082	0.2650	2.5193	31.5	(215)	0.0011
	41.0277	0.3131	2.1981	27.1	(224)	0.0013
	43.2196	0.3131	2.0916	27.3	(029)	0.0013
	49.6026	0.3132	1.8364	27.9	(0211)	0.0012
	54.1790	0.4335	1.6915	20.6	(236)	0.0017
	57.0213	0.4335	1.6138	20.9	(1114)	0.0017
	62.5853	0.5299	1.4830	17.5	(3012)	0.0020
4	24.1734	0.2439	3.6788	33.3	(114)	0.0010
	30.2168	0.3523	2.9553	23.4	(211)	0.0015
	33.2520	0.2710	2.6922	30.6	(124)	0.0011
	35.5014	0.4065	2.5266	20.5	(215)	0.0017
	40.9485	0.4336	2.2022	19.6	(224)	0.0018
	49.4309	0.4607	1.8423	19.0	(0211)	0.0018
	54.0108	0.5420	1.6964	16.5	(236)	0.0021
	56.8293	0.5420	1.6188	16.7	(1114)	0.0021
	62.4661	0.6233	1.4856	14.9	(3012)	0.0023
5	30.1355	0.3794	2.9631	21.7	(211)	0.0016
	33.2249	0.3794	2.6943	21.9	(124)	0.0016
	35.5285	0.4065	2.5247	20.5	(215)	0.0017
	40.8672	0.4065	2.2064	20.9	(224)	0.0017
	49.3767	0.4878	1.8442	17.9	(320)	0.0019
	54.0108	0.4336	1.6964	20.6	(236)	0.0017
	56.8564	0.4065	1.6181	22.2	(1114)	0.0016
	62.4390	0.5420	1.4862	17.1	(3012)	0.0020
6	33.1707	0.4607	2.6986	18.0	(124)	0.0019
	35.5285	0.4607	2.5247	18.1	(215)	0.0019
	40.8401	0.3794	2.2078	22.3	(224)	0.0016
	54.0921	0.4065	1.6941	21.9	(236)	0.0016
	56.8293	0.4336	1.6188	20.8	(1114)	0.0017
	62.4119	0.5149	1.4867	18.0	(3012)	0.0019

The experimental XRD data were further used to study the structural properties. The lattice constants (a) and (c) for the calcium phosphate tetragonal structure were calculated using the two peaks of directions (215), and (3012) according to the equation

$$\frac{1}{d_{hkl}^2} = \frac{h^2+k^2}{a^2} + \frac{l^2}{c^2}$$

Then by substituting $\frac{1}{d_{hkl}^2} = \frac{4sin^2\theta_{hkl}}{n^2\lambda^2}$ from the Bragg law can written as:

$$Sin^2\theta_{hkl} = A(h^2 + k^2) + Cl^2 \quad \text{where: A=}\lambda^2/4a^2 \text{, C=}\lambda^2/4c^2$$

$$Sin^2(35.60)= 5A + 25C \quad \text{............1}$$

$$Sin^2(62.58)= 9A + 144C \quad \text{............2}$$

Solving the two equations for the two selected lines can measure the lattice constants. Table 3.3 illustrates the lattice constants for calcium phosphate layers deposited at different Ca/P ratios and different distances. The calculated lattice constants values are nearly equal to the previous calculated ones. The lowest a and c values were appeared at a 1.65 ratio, while it increased with increasing the distance to 4 cm and they reduced for more distance.

Table 3.3: Lattice constants for calcium phosphate layers deposited at different Ca/P ratios and different distances.

Ca/P	a	c
1.4	6.6425	24.0578
1.5	6.6309	24.0422
1.65	6.6497	24.0911
1.8	6.6653	24.0258
1.9	6.6745	24.2458
D(cm)	a	c
2	6.6155	24.0229
3	6.6497	24.0911
4	6.6600	24.1339
5	6.6340	24.1344
6	6.6288	24.1489

3.3 FTIR Spectroscopy

The study of the functional groups of the deposited layer by FTIR gives a clear picture of the composition of the bonding molecules and the formation of the required compounds. Calcium phosphate compounds have many bonds that strongly absorb in the infrared spectrum. Determination depends on several variables depending on the preparation conditions, but despite these variables, the values remain very similar for all samples as shown in Figures 3.3 and 3.4 for samples prepared in different Ca/P ratios.

Two bands of phosphate groups were appeared, each one divided into three peaks at about 1082.69, 1019.29, 903.03 cm^{-1}, and another at 579.65, 539.49, 471.86 cm^{-1}, which belongs to the calcium phosphate structure [142,143]. Phosphate ions have multiple vibrational modes due to the multiple degrees of freedom. All these patterns appear at the infrared spectrum of the bones tissue and synthetic calcium phosphate . The examinations also confirmed that the samples contained carbonate ions with the appearance of the bands at 1412.42, 1082.69, and 805.81 cm^{-1} [145] comes from using the flammable gas in deposition process. In addition, the OH bands appeared at 3400, 1640.69, and 645.17 cm^{-1}, corresponding to adsorbed water molecules on the samples surface.

The carbonate bands are shown to be of high intensity compared to the phosphate bands which indicates the high carbonate content in all samples. The phosphate peaks are the most obvious in the prepared sample with a ratio of Ca/P = 1.65 compared to other samples that are less clear and some of them gradually disappear by moving away from this ratio. The energy of the bonds varies according to the ratio, as the two central peaks of phosphate appeared with the highest values at the 1.65 ratio.

In addition to the above-mentioned bonds for each of the Amide I, Amide II and Amide III. Table 3.4 shows the bands of the infrared spectrum for the five samples at different Ca/P ratios.
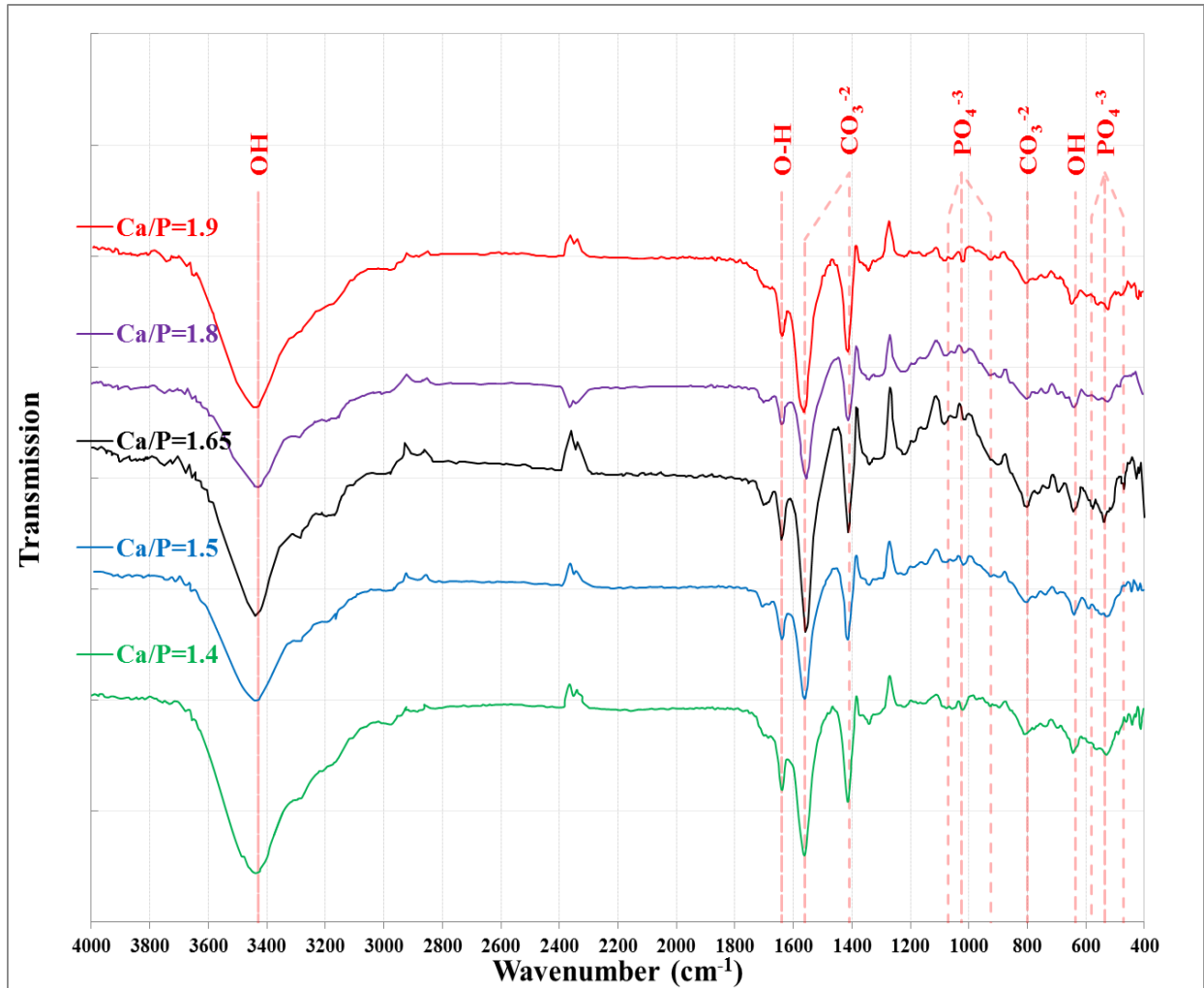

Figure 3.3: FTIR patterns from 400 to 4000 cm^{-1} for calcium phosphate layers deposited at different Ca/P ratios.
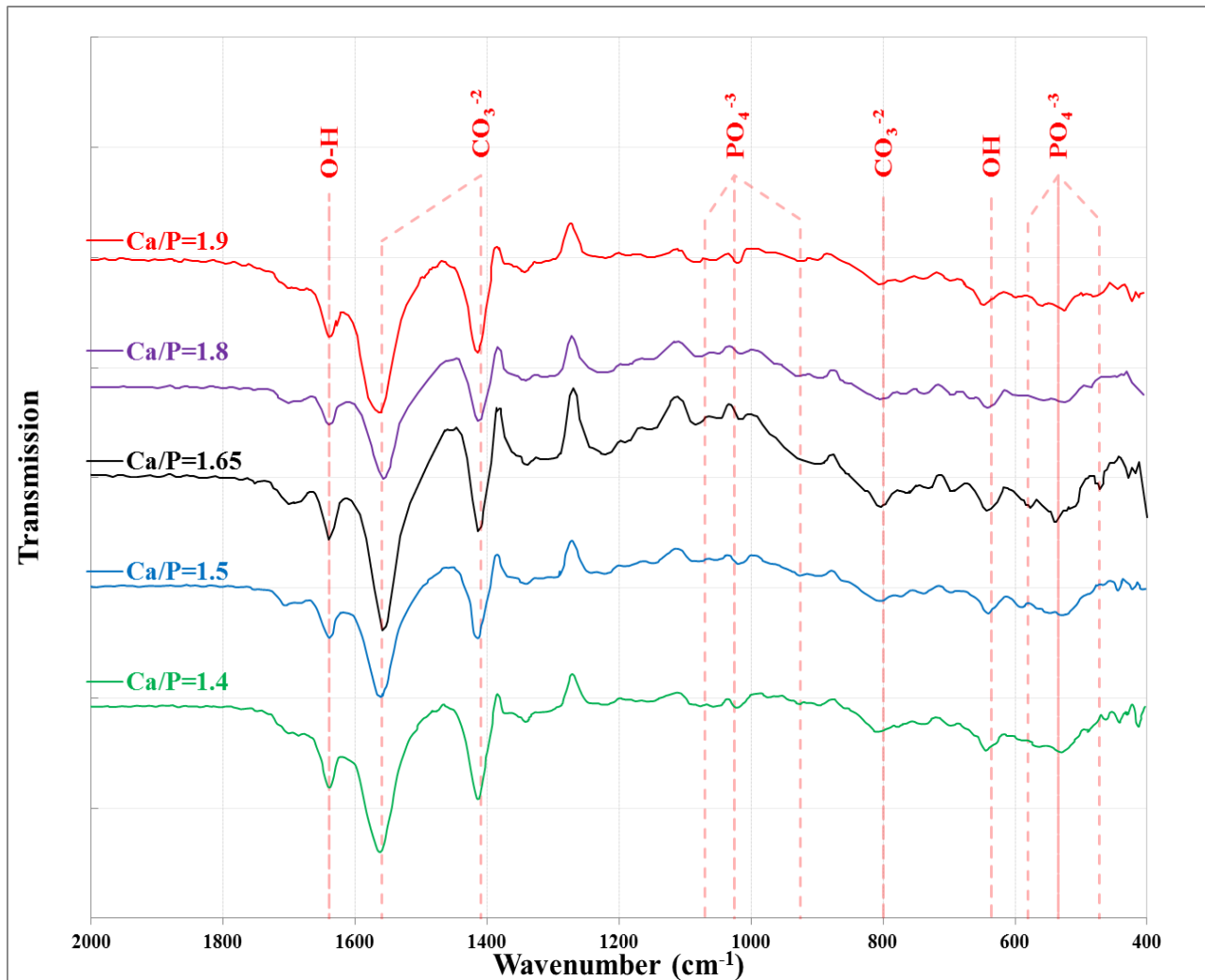
Figure 3.4: FTIR patterns of calcium phosphate layers deposited at different Ca/P ratios.

Table 3.4: FTIR bands of calcium phosphate layers deposited at different Ca/P ratios.

Band type	Wavenumber (cm^{-1}) Ca/P ratio				
	1.4	**1.5**	**1.65**	**1.8**	**1.9**
O-H	1638.57	1640.69	1640.69	1640.69	1640.69
CO$_3$$^{-2}$	1562.48	1564.60	1558.26	1558.26	1566.71
	1414.53	1416.64	1412.42	1414.53	1414.53
PO$_4$$^{-3}$	1076.35	-	1082.69	1074.24	1082.69
	1021.40	1021.40	1023.29	1021.40	1021.40
	924.17	928.40	935. 03	-	924.17
CO$_3$$^{-2}$	810.04	805.81	805.81	803.69	805.81
OH	647.29	643.07	645.17	643.06	649.40
PO$_4$$^{-3}$	-	592.34	579.65	-	560.63
	533.16	526.82	539.49	524.70	524.70
	463.41	-	471.86	484.54	476.09

Figures 3.5 shows the FTIR patterns for calcium phosphate layers of Ca/P ratio = 1.65 deposited at different distances. Nearly the same bands appeared in all samples as mentioned in the previous section. The fingerprint of phosphate groups bands disappeared gradually with increasing the distance 3cm from the flame orifice. Table 3.5 displays the bands of the infrared spectrum for the Ca/P= 1.65 deposited at different distances.
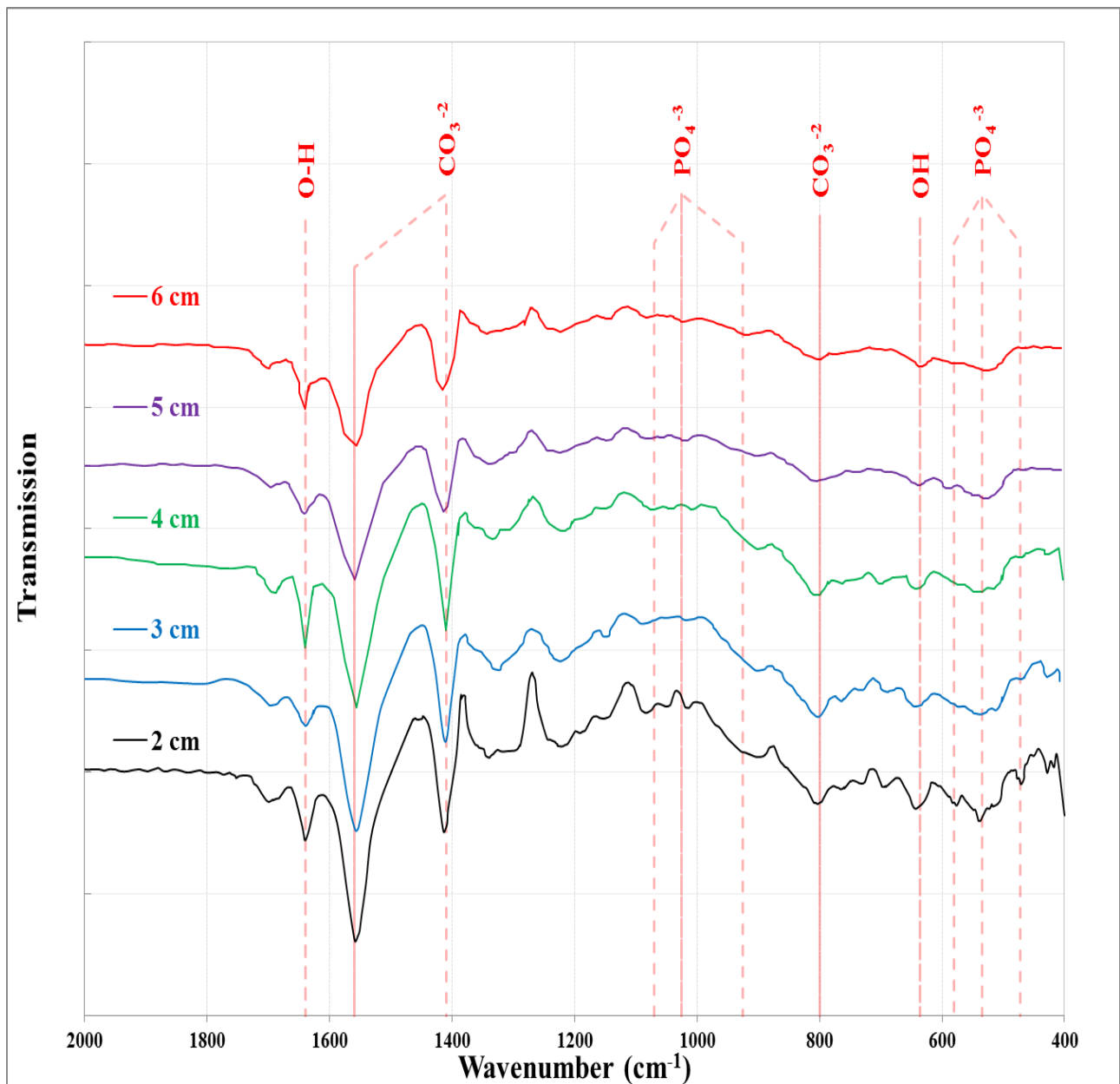

Figure 3.5: FTIR patterns for calcium phosphate layers deposited at different distances.

Table 3.5: FTIR bands in calcium phosphate layers deposited at different distances.

Band type	Wavenumber (cm^{-1}) Distance from flame orifice (cm)				
	2	**3**	**4**	**5**	**6**
O-H	1640.69	1640.69	1640.69	1642.8	1640.69
CO$_3^{-2}$	1558.26	1558.26	1556.14	1560.37	1560.37
	1412.42	1412.42	1410.30	1412.42	1416.64
PO$_4^{-3}$	1082.69	-	1072.13	1023.51	1023.51
	1019.29	1023.51	-	-	-
	903.03	907.26	905.15	-	-
CO$_3^{-2}$	805.81	805.81	805.81	801.58	805.81
OH	645.17	640.95	643.06	636.72	636.72
PO$_4^{-3}$	579.65	-	-	592.33	-
	539.49	539.49	535.61	533.15	526.81
	471.86	473.97	471.86	-	-

3.4 The Field Emission Scanning Electron Microscopy (FESEM)

The field emission scanning electron microscopy (FE-SEM) images show the nanostructure morphology. For each sample, we take two images in two different magnifications. The images at 35 kX magnification power showing the general shape, and other ones of 135 kX magnification focused on more details of nanostructure shapes and there dimensions. Figure 3.6 shows the FESEM images for coating prepared at different Ca/P ratios. The sample surfaces vary in shapes of nanostructures. At low Ca/P ratio the sample appeared of bulk coating and attached with some nanoparticles. These samples seemed with some cracks and low porosity. At high Ca/P ratio, as same as at the low ratio the coating appeared with low porosity and converted to smoothed surface at the highest ratio without any pores. The sample at 1.65 Ca/P ratio, which is nearly the stoichiometric ratio of hydroxyapatite in human bones, appeared as a distinctive sample of nanostructures of bumps shape of diameter about 317 nm, uniformly distributed forming high porosity structure.
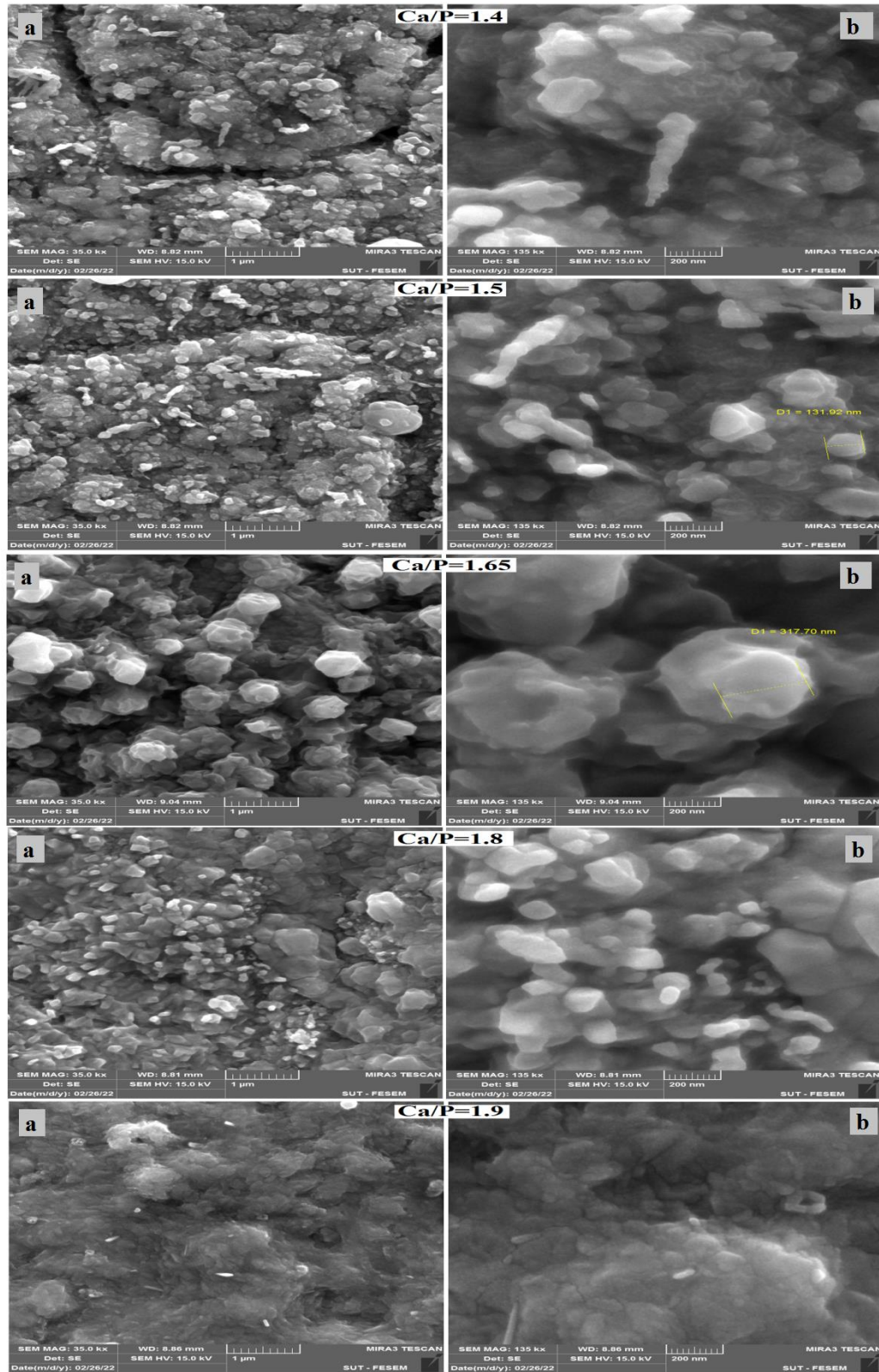
Figure 3.6: FE-SEM images for calcium phosphate layers deposited at different ratios

(a) magnification 35.0kx ,(b) magnification 135kx

Figure 3.7 shows the FE-SEM images for calcium phosphate coating prepared at 1.65 Ca/P ratio and at different distances from flame orifice. The surfaces behavior varies according to the distance. The deposition temperature differs depending on the distance from the flame orifice, where it is expected that the sample will be at a specific distance is deposited at a higher temperature. Therefore, the prepared sample appeared with a distance of 3 cm as a distinct deposited sample, while increasing the distance led to a decrease in the growth efficiency, so the surface of the samples appeared smooth.
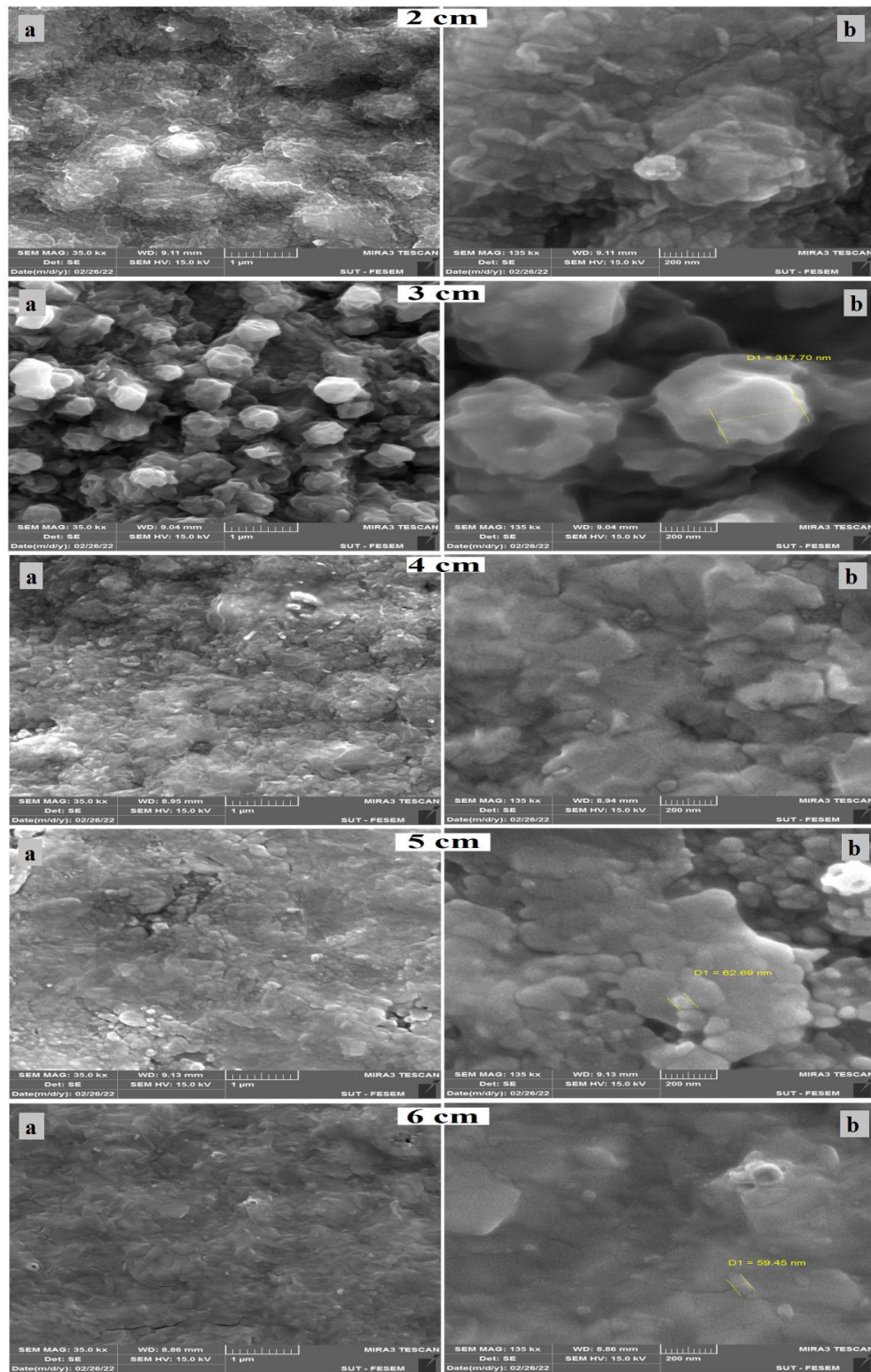
Figure 3.7: FE-SEM images for calcium phosphate layers deposited at different distances

(a) magnification 35.0kx ,(b) magnification 135kx

3.5 Energy Dispersive X-Ray Spectroscopy (EDX)

Figure 3.8 shows EDX patterns for calcium phosphate samples deposited at different ratios. We note that P element at 1.4 Ca/P ratio and it is gradually decreases in the other ratios. The other elements (Fe, Ni and Cr) appeared in all samples corresponding to the stainless steel (SS) substrate. The Au comes from coating of sample prior the testing by FE-SEM to enhance the image resolution.
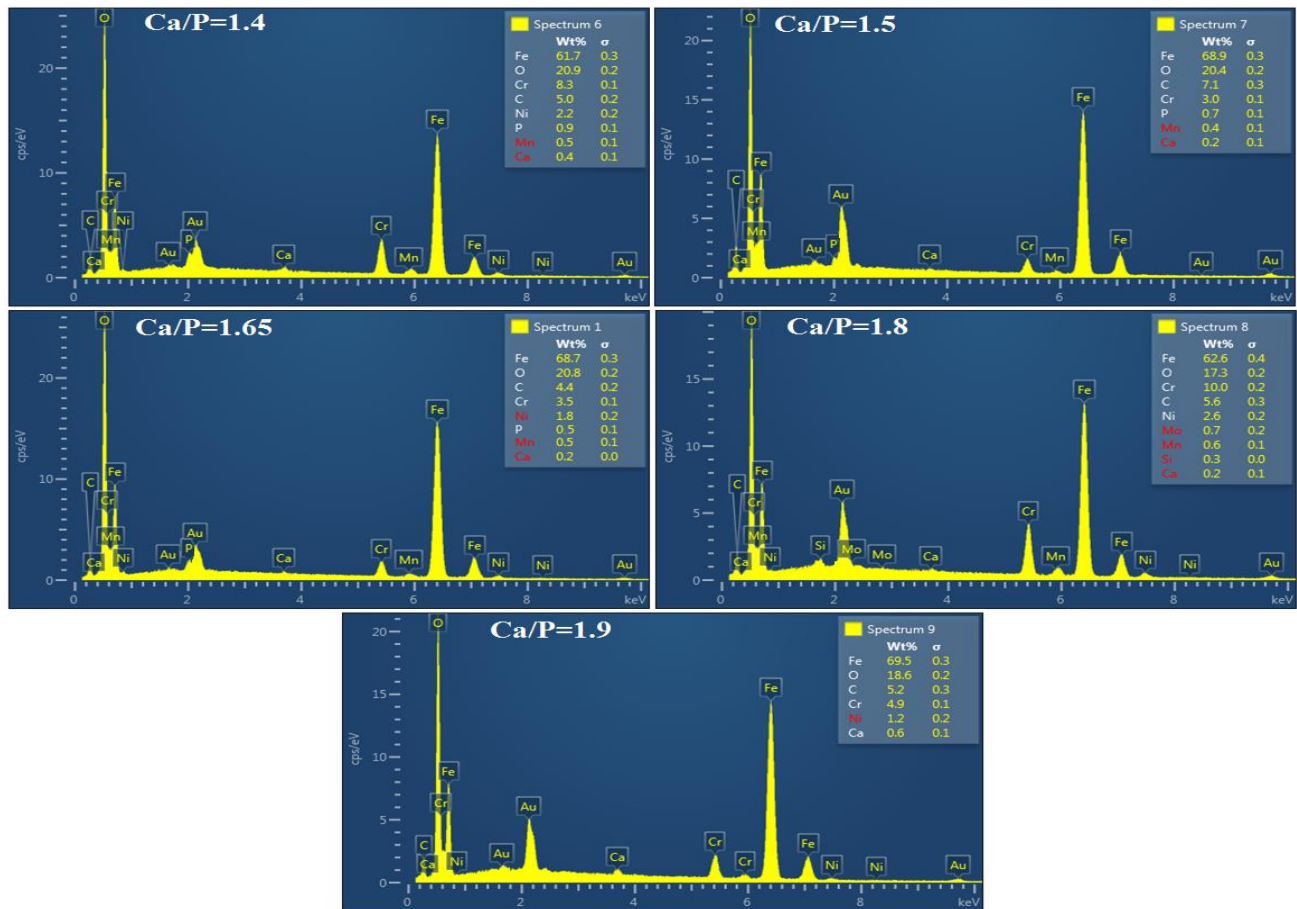

Figure 3.8 : EDX analysis for calcium phosphate layers deposited at different ratios.

Figure 3.9 shows the calcium phosphate layer deposited on stainless steel (SS) substrates at different distances and constant Ca/P ratio of 1.65. It is note that the substrate elements line varies according to coating covering.
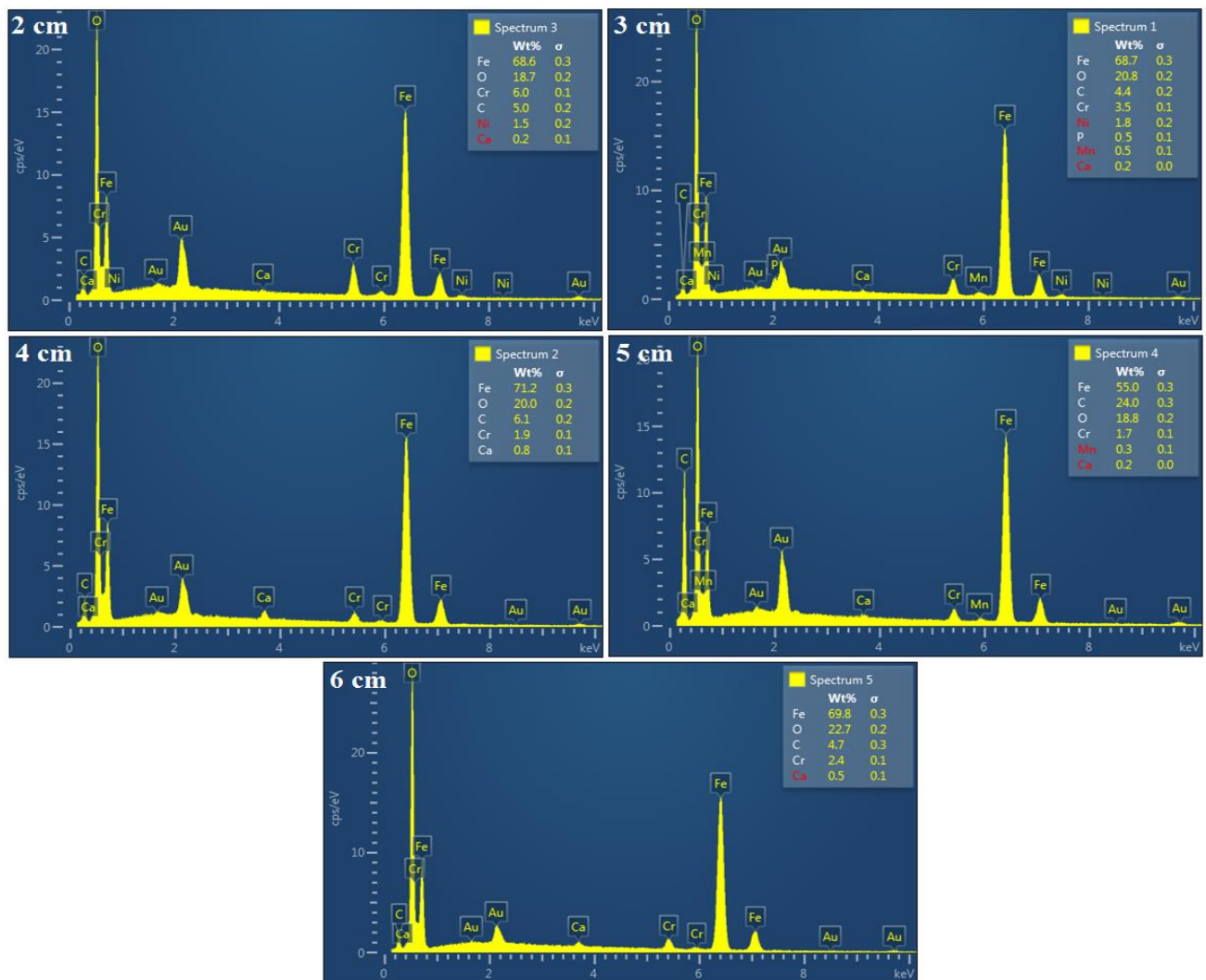
Figure 3.9: EDX analysis for calcium phosphate layers deposited at different distances.

3.6 Structural properties after Immersing in simulated body fluid (SBF)

Figure 3.10 shows the XRD patterns for the calcium phosphate layers at different Ca/P ratios, on stainless steel (SS) substrates, after immersing in simulated body fluid (SBF) to examine the samples biocompatibility. All samples showed polycrystalline calcium phosphate for the started coating and additional peaks corresponding to the hydroxyapatite phase specially for the sample prepared at 1.65 ratio of highest

crystalline hydroxyapatite (HA) phase. The characteristics peaks for the HAp phase at 2θ= 25.8 ,31.8, and 33.2º corresponding to (002), (211), and (300) planes, respectively for matched with the standard card ICDD No. 96-901-3628. This result indicate this sample candidate for use in implants to accelerate bone heeling.
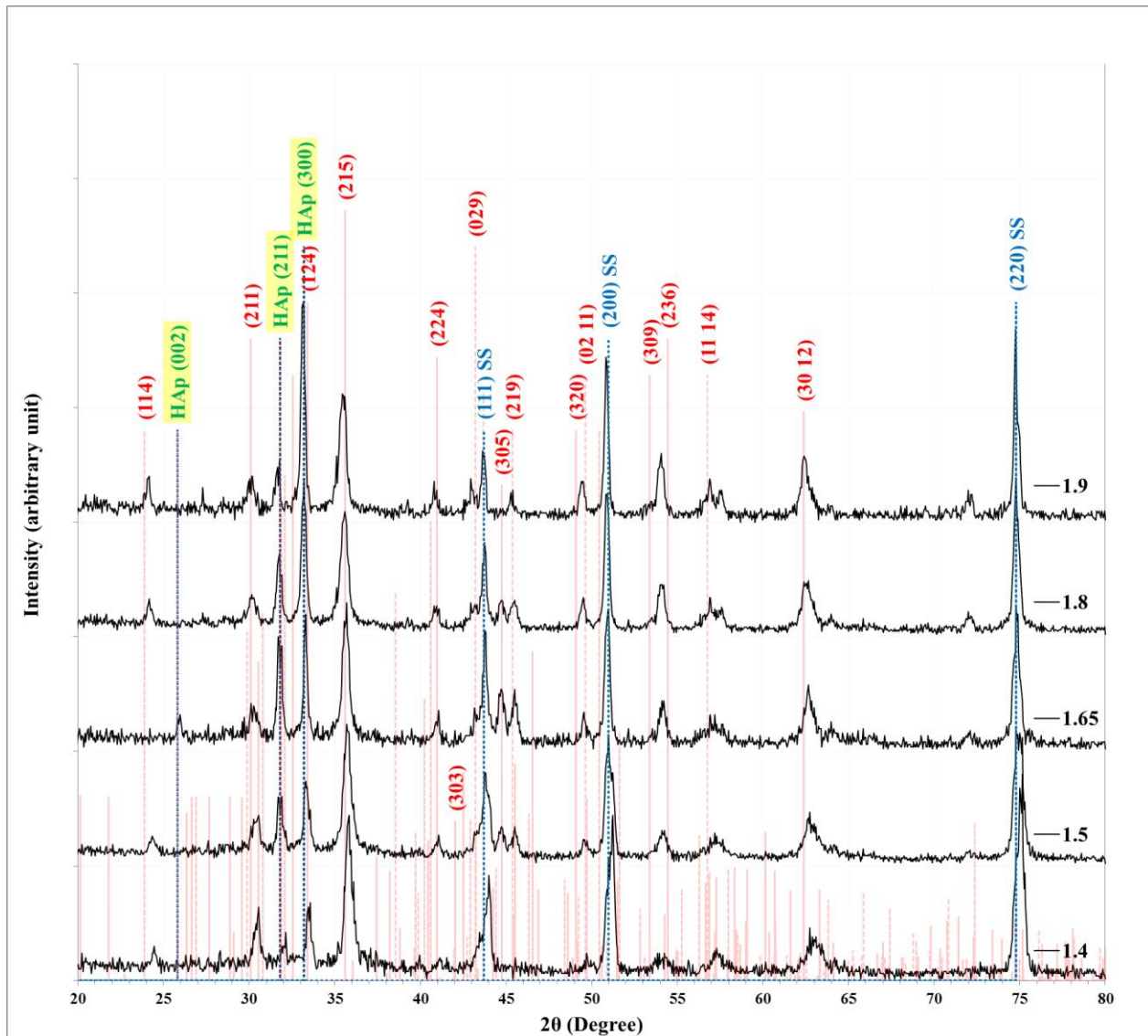

Figure 3.10: XRD patterns for the stainless steel (SS) slides coated with calcium phosphate layers at different Ca/P ratios after immersing in SBF for 21 days.

3.7 Antibacterial Activity of the Prepared Samples

Figure 3.11 shows the antibacterial activity test of the prepared calcium phosphate samples on SS substrates by flame coating at different Ca/P ratios at 3 cm from the flame orifice using diffusion disc procedure. 5×5 mm^2 SS samples coated with the calcium phosphate layers over the agar surface spread with *E.Coli* bacteria and incubated for 24 hours at 37 ℃. The bacteria are grown over the entire agar instead of some areas around some samples.

No inhibition around the control sample and the sample prepared at 1.4 and 1.9 Ca/P ratios, while 9, 11, and 10 mm inhibition zone diameter around the samples prepared 1.5, 1.65, and 1.8, respectively. So the highest antibacterial effect appeared for sample prepared at the 1.65 Ca/P ratio.

The antibacterial activity of nanoparticles depend on different mechanism : the first is to alter cell membrane permeability cause to loose major of the bacterial liquid causing its death; the second is to inhibit the ribosome subunit for the RNA binding with the nanoparticles accumulated within the bacteria, causing a collapse of biological process. Furthermore, the nanoparticles can produce reactive species (ROS) cause bacterial death with special actions [146].
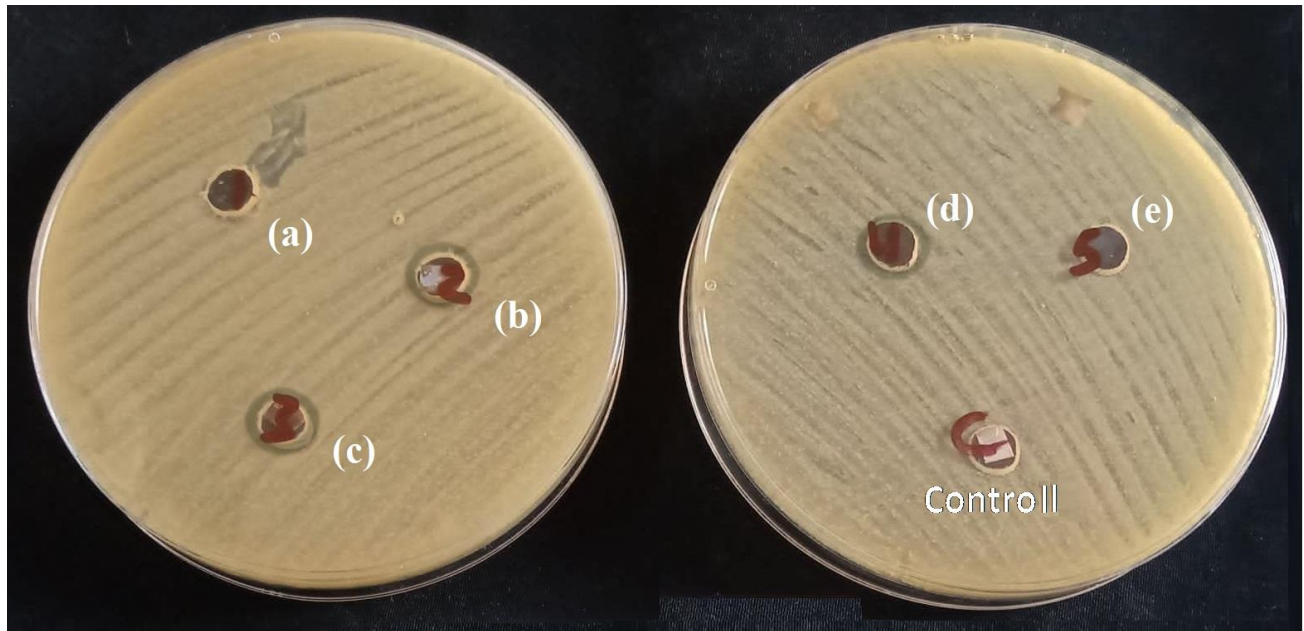
Figure 3.11: Antibacterial Activity for the calcium phosphate layers on SS slides at different (a) 1.4, (b) 1.5, (c) 1.65, (d) 1.8, and (e) 1.9 Ca/P ratios compared with uncoated substrate against E. Coli bacteria in the table.

3.8 Conclusions

1. A method in which biocompatible layers was built from a simple, locally available, one-step technique, and low cost.

2. The tests showed the deposited layers have a good properties that can be used to cover the medical implant to reduce the healing period.

3. The X-ray diffraction showed the crystal structure identical to calcium phosphite, and the best crystallization was at a ratio of 1.65 and at a distance of 3 cm.

4. FESEM images showed that the sample with the same ratio possesses a distinctive composition as the surface had a high porosity on which bone could be built easily.

5. The FTIR test showed the distinctive bonds of calcium phosphite and a slight change from one sample to another. The best samples were in the same ratio, as the bands were distinct in this ratio.

6. Examinations of the simulated body fluid showed the growth of a hydroxyapatite layer, which was confirmed by X-ray examinations, which indicate the implant coated with these layers can accelerate the process of bone building on these layers and the connection of bone tissue with medical implant.

7. Examinations antibacterial showed that they prevent the growth of bacteria on them, which enhance the process of using them as medical implant.

3.9 Suggestions for Future Work

1. Deposition testing of biocompatible layers on different substrates.

2. Testing bio-layers with different doping.

3. Determine the toxicity of the deposited layers to ensure its use in medical

   implants.

References

[1] Martin, P. M. (2009). Handbook of deposition technologies for films and coatings: science, applications and technology. William Andrew.

[2] Griesser, H. J. (2016). Thin film coatings for biomaterials and biomedical applications.

[3] Mozafari, M., Ramedani, A., Zhang, Y. N., & Mills, D. K. (2016). Thin films for tissue engineering applications. In Thin Film Coatings for Biomaterials and Biomedical Applications (pp. 167–195). Elsevier.

[4] Driver, M. (2012). Coatings for biomedical applications. Elsevier.

[5] Piedade, A. P., Romeu, F., Branco, R., & Morais, P. V. (2018). Thin films for medical and environmental applications. In Methods for Film Synthesis and Coating Procedures. IntechOpen.

[6] Wu, Z., Huang, Y., & Chen, R. (2017). Opportunities and challenges in flexible and stretchable electronics: A panel discussion at ISFSE2016. Multidisciplinary Digital Publishing Institute.

[7] Chopra, K. N. (2012). A Technical Review on the Thin-Films Coatings for Enhancing the Efficiency of the Photo-Voltaic Cells for Solar Energy Applications. Invertis Journal of Renewable Energy, 2(4), 199–207.

[8] Tavares, J., Swanson, E. J., & Coulombe, S. (2008). Plasma synthesis of coated metal nanoparticles with surface properties tailored for dispersion. Plasma Processes and Polymers, 5(8), 759–769.

[9] Hanaor, D. A. H., Triani, G., & Sorrell, C. C. (2011). Morphology and photocatalytic activity of highly oriented mixed phase titanium dioxide thin films. Surface and Coatings Technology, 205(12), 3658–3664.

[10] Das, B. K. (2021). Growth of ZnO thin film on silicon and glass substrate by pulsed laser deposition technique. Available at SSRN 3840984.

[11] Tappa, K., & Jammalamadaka, U. (2018). Novel biomaterials used in medical 3D printing techniques. Journal of Functional Biomaterials, 9(1), 17.

[12] Park, J. B., & Bronzino, J. D. (2000). The biomedical engineering handbook. Boca Raton, FL: CRC Press, 4, 1–8.

[13] Zhu, S. L., Wang, X. M., Qin, F. X., & Inoue, A. (2007). A new Ti-based bulk glassy alloy with potential for biomedical application. Materials Science and Engineering: A, 459(1–2), 233–237.

[14] Devi, A. V. G., Rajendran, V., & Rajendran, N. (2010). Structure, solubility and bioactivity in TiO2-doped phosphate-based bioglasses and glass–ceramics. Materials Chemistry and Physics, 124(1), 312–318.

[15] Helmus, M. N., Gibbons, D. F., & Cebon, D. (2008). Biocompatibility: meeting a key functional requirement of next-generation medical devices. Toxicologic Pathology, 36(1), 70–80.

[16] Pramanik, S., Agarwal, A. K., & Rai, K. N. (2005). Chronology of total hip joint replacement and materials development. Trends in Biomaterials & Artificial Organs, 19(1), 15–26.

[17] Ghasemi-Mobarakeh, L., Kolahreez, D., Ramakrishna, S., & Williams, D. (2019). Key terminology in biomaterials and biocompatibility. Current Opinion in Biomedical Engineering, 10, 45–50.

[18] Williams, D. F. (2008). On the mechanisms of biocompatibility. Biomaterials, 29(20), 2941–2953.

[19] Tappa, K., & Jammalamadaka, U. (2018). Novel biomaterials used in medical 3D printing techniques. Journal of Functional Biomaterials, 9(1), 17.

[20] Kamachimudali, U., Sridhar, T. M., & Raj, B. (2003). Corrosion of bio implants. Sadhana, 28(3), 601–637.

[21] Lee, H. B., Khang, G., & Lee, J. H. (2007). Polymeric biomaterials. Biomaterials, 1–3.

[22] Atala, A., Lanza, R., Mikos, T., & Nerem, R. M. (Eds.). (2018). Principles of regenerative medicine. Academic press.

[23] Ehrlich, H. (2010). Biological materials of marine origin .New York, NY, USA: Springe (pp. 1-436).

[24] Albertsson, A. C., & Varma, I. K. (2002). Aliphatic polyesters: Synthesis, properties and applications. Degradable aliphatic polyesters, 1-40.

[25] Parida, P., Behera, A., & Mishra, S. C. (2012). Classification of Biomaterials used in Medicine.

[26] Hussein, M. A., Mohammed, A. S., & Al-Aqeeli, N. (2015). Wear Characteristics of Metallic Biomaterials: A Review. Materials 8, 2749–2768.

[27] Raghavendra, G. M., Varaprasad, K., & Jayaramudu, T. (2015). Biomaterials: design, development and biomedical applications. In Nanotechnology applications for tissue engineering (pp. 21–44). Elsevier.

[28] Najeeb, S., Khurshid, Z., Ghabbani, H., Zafar, M. S., & Sefat, F. (2019). Nano glass ionomer cement: modification for biodental applications. In Advanced Dental Biomaterials (pp. 217–227). Elsevier.

[29] Sendax, V. D. (2012). Mini dental implants: principles and practice. Elsevier Health Sciences.

[30] Çınar, İ. Ç., Gültekin, B. A., Sağlanmak, A., & Töre, C. (2020). Dental Implants. In Biomaterials. IntechOpen.

[31] Hoeppner, D. W., & Chandrasekaran, V. (1994). Fretting in orthopaedic implants: a review. Wear, 173(1–2), 189–197.

[32] Ratner, B. D., Hoffman, A. S., Schoen, F. J., & Lemons, J. E. (2004). Biomaterials science: an introduction to materials in medicine. Elsevier.

[33] Narayan, R. (2012). Fundamentals of medical implant materials. ASM Handbook.

[34] Davies, J. E., Ottensmeyer, P., Shen, X., Hashimoto, M., & Peel, S. A. F. (2016). 20. Early Extracellular Matrix Synthesis by Bone Cells. In Bone-Bio Material Interface (pp. 214–228). University of Toronto Press.

[35] Ducheyne, P., Radin, S., & King, L. (1993). The effect of calcium phosphate ceramic composition and structure on in vitro behavior. I. Dissolution. Journal of Biomedical Materials Research, 27(1), 25–34.

[36] Ibrahim, M. Z., Sarhan, A. A. D., Yusuf, F., & Hamdi, M. (2017). Biomedical materials and techniques to improve the tribological, mechanical and biomedical properties of orthopedic implants–A review article. Journal of Alloys and Compounds, 714, 636–667.

[37] Long, M., & Rack, H. J. (1998). Titanium alloys in total joint replacement—a materials science perspective. Biomaterials, 19(18), 1621–1639.

[38] Malekani, J., Schmutz, B., Gu, Y., Schuetz, M., & Yarlagadda, P. (2011). Biomaterials in orthopedic bone plates: a review. Proceedings of the Annual International Conference on Materials Science, Metal and Manufacturing, 71–76.

[39] Chen, X. H., Lu, J., Lu, L., & Lu, K. (2005). Tensile properties of a nanocrystalline 316L austenitic stainless steel. Scripta Materialia, 52(10), 1039–1044.

[40] Chen, Q., Liu, A., Qiu, H., & Yang, Y. (2015). Mesenchymal stem cell and endothelial cell interaction restores endothelial permeability via paracrine hepatocyte growth factor in vitro. Critical Care, 19(1), 1–201.

[41] Hedberg, Y., Karlsson, M.-E., Blomberg, E., Wallinder, I. O., & Hedberg, J. (2014). Correlation between surface physicochemical properties and the release of iron from stainless steel AISI 304 in biological media. Colloids and Surfaces B: Biointerfaces, 122, 216–222.

[42] Hedberg, Y., Wang, X., Hedberg, J., Lundin, M., Blomberg, E., & Wallinder, I. O. (2013). Surface-protein interactions on different stainless steel grades: effects of protein adsorption, surface changes and metal release. Journal of Materials Science: Materials in Medicine, 24(4), 1015–1033.

[43] Oh, S., Daraio, C., Chen, L., Pisanic, T. R., Finones, R. R., & Jin, S. (2006). Significantly accelerated osteoblast cell growth on aligned TiO2 nanotubes. Journal of Biomedical Materials Research Part A: An Official Journal of The Society for Biomaterials, The Japanese Society for Biomaterials, and The Australian Society for Biomaterials and the Korean Society for Biomaterials, 78(1), 97–103.

[44] Patnaik, L., Maity, S. R., & Kumar, S. (2020). Status of nickel free stainless steel in biomedical field: A review of last 10 years and what else can be done. Materials Today: Proceedings, 26, 638–643.

[45] Trelewicz, J. R., Halada, G. P., Donaldson, O. K., & Manogharan, G. (2016). Microstructure and corrosion resistance of laser additively manufactured 316L stainless steel. Jom, 68(3), 850–859.

[46] Man, C., Dong, C., Liu, T., Kong, D., Wang, D., & Li, X. (2019). The enhancement of microstructure on the passive and pitting behaviors of selective laser melting 316L SS in simulated body fluid. Applied Surface Science, 467, 193–205.

[47] Harun, W. S. W., Asri, R. I. M., Romlay, F. R. M., Sharif, S., Jan, N. H. M., & Tsumori, F. (2018). Surface characterisation and corrosion behaviour of oxide layer for SLMed-316L stainless steel. Journal of Alloys and Compounds, 748, 1044–1052.

[48] Lodhi, M. J. K., Deen, K. M., Greenlee-Wacker, M. C., & Haider, W. (2019). Additively manufactured 316L stainless steel with improved corrosion resistance and biological response for biomedical applications. Additive Manufacturing, 27, 8–19.

[49] Goodman, S. B., Yao, Z., Keeney, M., & Yang, F. (2013). The future of biologic coatings for orthopaedic implants. Biomaterials, 34(13), 3174–3183.

[50] Ribeiro, M., Monteiro, F. J., & Ferraz, M. P. (2012). Infection of orthopedic implants with emphasis on bacterial adhesion process and techniques used in studying bacterial-material interactions. Biomatter, 2(4), 176–194.

[51] Sudhakar, K. V, & Wang, J. (2011). Fatigue behavior of Vitallium-2000 Plus alloy for orthopedic applications. Journal of Materials Engineering and Performance, 20(6), 1023–1027.

[52] Manivasagam, G., Dhinasekaran, D., & Rajamanickam, A. (2010). Biomedical implants: corrosion and its prevention-a review. Recent Patents on Corrosion Science.

[53] Hanumantharaju, H. G., Shivananda, H. K., Hadimani, M. G., Kumar, K. S., & Jagadish, S. P. (2000). Wear study on SS316L, Ti-6Al-4V, PEEK, polyurethane and alumina used as bio-material. Wear, 2000, 0.

[54] Hermawan, H., Ramdan, D., & Djuansjah, J. R. P. (2011). Metals for biomedical applications. Biomedical Engineering-from Theory to Applications, 1, 411–430.

[55] Kowolik, J., Kozlowski, D., & Jones, J. E. (2007). Utilization of stainless steel crowns by general dentists and pediatric dental specialists in Indiana. Journal (Indiana Dental Association), 86(2), 16–21.

[56] Balani, K., Anderson, R., Laha, T., Andara, M., Tercero, J., Crumpler, E., & Agarwal, A. (2007). Plasma-sprayed carbon nanotube reinforced hydroxyapatite coatings and their interaction with human osteoblasts in vitro. Biomaterials, 28(4), 618–624.

[57] Hench, L. L. (1998). Bioceramics, a clinical success. American Ceramic Society Bulletin, 77(7), 67–74 .

[58] Li, P., & De Groot, K. (1993). Calcium phosphate formation within sol-gel prepared titania in vitro and in vivo. Journal of Biomedical Materials Research, 27(12), 1495–1500.

[59] Ben-Nissan, B., & Green, D. W. (2014). Marine structures as templates for biomaterials. In Advances in calcium phosphate biomaterials (pp. 391–414). Springer.

[60] Kuriakose, T. A., Kalkura, S. N., Palanichamy, M., Arivuoli, D., Dierks, K., Bocelli, G., & Betzel, C. (2004). Synthesis of stoichiometric nano crystalline hydroxyapatite by ethanol-based sol–gel technique at low temperature. Journal of Crystal Growth, 263(1–4), 517–523.

[61] Chavan, P. N., Bahir, M. M., Mene, R. U., Mahabole, M. P., & Khairnar, R. S. (2010). Study of nanobiomaterial hydroxyapatite in simulated body fluid: Formation and growth of apatite. Materials Science and Engineering: B, 168(1–3), 224–230.

[62] Kokubo, T., & Takadama, H. (2006). How useful is SBF in predicting in vivo bone bioactivity? Biomaterials, 27(15), 2907–2915.

[63] Davies, J. E., Ottensmeyer, P., Shen, X., Hashimoto, M., & Peel, S. A. F. (2016). 20. Early Extracellular Matrix Synthesis by Bone Cells. In Bone-Bio Material Interface (pp. 214–228). University of Toronto Press.

[64] Agrawal, K., Singh, G., Puri, D., & Prakash, S. (2011). Synthesis and characterization of hydroxyapatite powder by sol-gel method for biomedical application. Journal of Minerals & Materials Characterization & Engineering, 10(8), 727–734.

[65] Radin, S. R., & Ducheyne, P. (1993). The effect of calcium phosphate ceramic composition and structure on in vitro behavior. II. Precipitation. Journal of Biomedical Materials Research, 27(1), 35–45.

[66] Prendergast, P. J., Huiskes, R., & Søballe, K. (1997). Biophysical stimuli on cells during tissue differentiation at implant interfaces. Journal of Biomechanics, 30(6), 539–548.

[67] Misch, C. E., Steigenga, J., Barboza, E., Misch-Dietsh, F., Cianciola, L. J., & Kazor, C. (2006). Short dental implants in posterior partial edentulism: a multicenter retrospective 6-year case series study. Journal of Periodontology, 77(8), 1340–1347.

[68] Alsaadi, G., Quirynen, M., Komárek, A., & Van Steenberghe, D. (2007). Impact of local and systemic factors on the incidence of oral implant failures, up to abutment connection. Journal of Clinical Periodontology, 34(7), 610–617.

[69] Alsaadi, G., Quirynen, M., Komárek, A., & Van Steenberghe, D. (2007). Impact of local and systemic factors on the incidence of oral implant failures, up to abutment connection. Journal of Clinical Periodontology, 34(7), 610–617.

[70] Geipel, U. (2009). Pathogenic organisms in hip joint infections. International Journal of Medical Sciences, 6(5), 234

[71] Campoccia, D., Montanaro, L., & Arciola, C. R. (2006). The significance of infection related to orthopedic devices and issues of antibiotic resistance. Biomaterials, 27(11), 2331–2339.

[72] Andrea, A., Molchanova, N., & Jenssen, H. (2018). Antibiofilm peptides and peptidomimetics with focus on surface immobilization. Biomolecules, 8(2), 27.

[73] Lind, M., Overgaard, S., Bünger, C., & Søballe, K. (1999). Improved bone anchorage of hydroxyapatite coated implants compared with tricalcium-phosphate coated implants in trabecular bone in dogs. Biomaterials, 20(9), 803–808.

[74] Berndt, C. C., Hasan, F., Tietz, U., & Schmitz, K.-P. (2014). A review of hydroxyapatite coatings manufactured by thermal spray. Advances in Calcium Phosphate Biomaterials, 267–329.

[75] Surmenev, R. A., Surmeneva, M. A., & Ivanova, A. A. (2014). Significance of calcium phosphate coatings for the enhancement of new bone osteogenesis–a review. Acta Biomaterialia, 10(2), 557–579.

[76] Yeom, G. Y., Thornton, J. A., & Kushner, M. J. (1989). Cylindrical magnetron discharges. II. The formation of dc bias in rf-driven discharge sources. Journal of Applied Physics, 65(10), 3825–3832.

[77] Sobieszczyk, S., & Zielinski, A. (2008). Coatings in arthroplasty. Advances in Materials Science, 8(4), 35.

[78] LIu, D.-M., Chou, H. M., & Wu, J. D. (1994). Plasma-sprayed hydroxyapatite coating: effect of different calcium phosphate ceramics. Journal of Materials Science: Materials in Medicine, 5(3), 147–153.

[79] Yang, Y., Kim, K.-H., & Ong, J. L. (2005). A review on calcium phosphate coatings produced using a sputtering process—an alternative to plasma spraying. Biomaterials, 26(3), 327–337.

[80] Chu, P. K., Chen, J. Y., Wang, L. P., & Huang, N. (2002). Plasma-surface modification of biomaterials. Materials Science and Engineering: R: Reports, 36(5–6), 143–206.

[81] Azem, F. A., Eroglu, E. O., & Cakir, A. (2011). Synthesis and structural properties of sol–gel derived Si-substituted hydroxyapatite coatings. Journal of Biomechanics, 44, 13.

[82] Choi, A. H., & Ben-Nissan, B. (2007). Sol-gel production of bioactive nanocoatings for medical applications. Part II: current research and development.

[83] Qu, H., & Wei, M. (2008). Improvement of bonding strength between biomimetic apatite coating and substrate. Journal of Biomedical Materials Research Part B: Applied Biomaterials: An Official Journal of The Society for Biomaterials, The Japanese Society for Biomaterials, and The Australian Society for Biomaterials and the Korean Society for Biomaterials, 84(2), 436–443.

[84] Ballarre, J., Seltzer, R., Mendoza, E., Orellano, J. C., Mai, Y.-W., García, C., & Ceré, S. M. (2011). Morphologic and nanomechanical characterization of bone tissue growth around bioactive sol–gel coatings containing wollastonite particles applied on stainless steel implants. Materials Science and Engineering: C, 31(3), 545–552.

[85] Rojaee, R., Fathi, M., Raeissi, K., & Sharifnabi, A. (2014). Biodegradation assessment of nanostructured fluoridated hydroxyapatite coatings on biomedical grade magnesium alloy. Ceramics International, 40(9), 15149–15158.

[86] Zhang, J. X., Guan, R. F., & Zhang, X. P. (2011). Synthesis and characterization of sol–gel hydroxyapatite coatings deposited on porous NiTi alloys. Journal of Alloys and Compounds, 509(13), 4643–4648.

[87] Strobel, R., Baiker, A., & Pratsinis, S. E. (2006). Aerosol flame synthesis of catalysts. Advanced Powder Technology, 17(5), 457–480.

[88] Teoh, W. Y., Amal, R., & Mädler, L. (2010). Flame spray pyrolysis: An enabling technology for nanoparticles design and fabrication. Nanoscale, 2(8), 1324–1347.

[89] Jodhani, G., & Gouma, P.-I. (2017). Flame spray pyrolysis processing to produce metastable phases of metal oxides. JOJ Material Science, 1, 1–5.

[90] Lengyel, M., Elhassid, D., Atlas, G., Moller, W. T., & Axelbaum, R. L. (2014). Development of a scalable spray pyrolysis process for the production of non-hollow battery materials. Journal of Power Sources, 266, 175–178.

[91] Kim, J. H., Yi, J. H., Ko, Y. N., & Kang, Y. C. (2012). Electrochemical properties of nano-sized $LiNi_{1/3}Co_{1/3}Mn_{1/3}O_2$ powders in the range from 56 to 101 nm prepared by flame spray pyrolysis. Materials Chemistry and Physics, 134(1), 254–259.

[92] Teoh, W. Y., Amal, R., & Mädler, L. (2010). Flame spray pyrolysis: An enabling technology for nanoparticles design and fabrication. Nanoscale, 2(8), 1324–1347.

[93] Carroz, J. W., Odencrantz, F. K., Finnegan, W. G., & Drehmel, D. C. (1980). Aerosol generation to simulate specific industrial fine particle effluents. American Industrial Hygiene Association Journal, 41(2), 77–84.

[94] Purwanto, A., Wang, W.-N., & Okuyama, K. (2011). Flame spray pyrolysis. In Handbook of Atomization and Sprays (pp. 869–879). Springer.

[95] Teoh, W. Y., Amal, R., & Mädler, L. (2010). Flame spray pyrolysis: An enabling technology for nanoparticles design and fabrication. Nanoscale, 2(8), 1324–1347.

[96] Strobel, R., Baiker, A., & Pratsinis, S. E. (2006). Aerosol flame synthesis of catalysts. Advanced Powder Technology, 17(5), 457–480.

[97] Thakurdesai, M., Kulkarni, N., Chalke, B., & Mahadkar, A. (2011). SYNTHESIS OF CdSe FILMS BY ANNEALING OF Cd/Se BILAYER. Chalcogenide Letters, 8(3), 223–229.

[98] Sousa, M. G., Da Cunha, A. F., & Fernandes, P. A. (2014). Annealing of RF-magnetron sputtered SnS2 precursors as a new route for single phase SnS thin films. Journal of Alloys and Compounds, 592, 80–85.

[99] Tsay, C.-Y., Fan, K.-S., Chen, S.-H., & Tsai, C.-H. (2010). Preparation and characterization of ZnO transparent semiconductor thin films by sol–gel method. Journal of Alloys and Compounds, 495(1), 126–130.

[100] Akarapu, A. (2011). Surface property modification of copper by nanocomposite coating.

[101] Mushtaq, S., Ismail, B., Zeb, M. A., Kissinger, N. J. S., & Zeb, A. (2015). Low-temperature synthesis and characterization of Sn-doped Sb2S3 thin film for solar cell applications. Journal of Alloys and Compounds, 632, 723–728.

[102] Batool, A., Kanwal, F., Imran, M., Jamil, T., & Siddiqi, S. A. (2012). Synthesis of polypyrrole/zinc oxide composites and study of their structural, thermal and electrical properties. Synthetic Metals, 161(23–24), 2753–2758.

[103] Bedlovicová, Z., & Salayová, A. (2017). Green-Synthesized Silver Nanoparticles and Their Potential for Antibacterial Applications. Bacterial Pathogenesis and Antibacterial Control.

[104] Abdullaeva, Z. (2017). Characterization of nanoparticles after biological synthesis. In Synthesis of Nanoparticles and Nanomaterials (pp. 177–195). Springer.

[105] Moran, G. P., Coleman, D. C., & Sullivan, D. J. (2012). Candida albicans versus Candida dubliniensis: why is C. albicans more pathogenic? International Journal of Microbiology, 2012.

[106] Jalal, M., Ansari, M. A., Alzohairy, M. A., Ali, S. G., Khan, H. M., Almatroudi, A., & Siddiqui, M. I. (2019). Anticandidal activity of biosynthesized silver nanoparticles: effect on growth, cell morphology, and key virulence attributes of Candida species. International journal of nanomedicine, 14, 4667.

[107] Patel, M. (2020). Antimicrobial Paper Embedded with Nanoparticles as Spread-Breaker for Corona Virus. J. Environ. Life Sci, 6, 1–12.

[108] Fox, C. M. (2014). Electrochemical Synthesis of Silver Nanoparticles for Applications in Nitrate Detection, Catalysis and Antibacterial Activity. National University of Ireland, Maynooth (Ireland).

[109] Synnott, D. W. (2019). Microwave Synthesis and Characterisation of Zinc Sulfide Nanomaterials for Photocatalytic and Anti-Bacterial Applications.

[110] Paczosa, M. K., & Mecsas, J. (2016). Klebsiella pneumoniae: going on the offense with a strong defense. Microbiology and Molecular Biology Reviews, 80(3), 629–661.

[111] Tong, S. Y. C., Davis, J. S., Eichenberger, E., Holland, T. L., & Fowler Jr, V. G. (2015). Staphylococcus aureus infections: epidemiology, pathophysiology, clinical manifestations, and management. Clinical Microbiology Reviews, 28(3), 603–661.

[112] Percival, S. L., Chalmers, R., Embrey, M., Hunter, P. R., Sellwood, J., & Wyn-Jones, P. (2004). Microbiology of waterborne diseases. Elsevier academic press ^ eUK UK.

[113] Mocanu, A., Furtos, G., Rapuntean, S., Horovitz, O., Flore, C., Garbo, C., Danisteanu, A., Rapuntean, G., Prejmerean, C., & Tomoaia-Cotisel, M. (2014). Synthesis; characterization and antimicrobial effects of composites based on multi-

substituted hydroxyapatite and silver nanoparticles. Applied Surface Science, 298, 225–235.

[114] Brzozowski, M., Krukowska, Ż., Galant, K., Jursa-Kulesza, J., & Kosik-Bogacka, D. (2020). Genotypic characterisation and antimicrobial resistance of Pseudomonas aeruginosa strains isolated from patients of different hospitals and medical centres in Poland. BMC Infectious Diseases, 20(1), 1–9.

[115] Oyane, A. (2010). Development of apatite-based composites by a biomimetic process for biomedical applications. Journal of the Ceramic Society of Japan, 118(1374), 77–81.

[116] Chavan, P. N., Bahir, M. M., Mene, R. U., Mahabole, M. P., & Khairnar, R. S. (2010). Study of nanobiomaterial hydroxyapatite in simulated body fluid: Formation and growth of apatite. Materials Science and Engineering: B, 168(1–3), 224–230.

[117] Waterman, J., Pietak, A., Birbilis, N., Woodfield, T., Dias, G., & Staiger, M. P. (2011). Corrosion resistance of biomimetic calcium phosphate coatings on magnesium due to varying pretreatment time. Materials Science and Engineering: B, 176(20), 1756–1760.

[118] Oyane, A., Wang, X., Sogo, Y., Ito, A., & Tsurushima, H. (2012). Calcium phosphate composite layers for surface-mediated gene transfer. Acta Biomaterialia, 8(6), 2034–2046.

[119] Surmeneva, M. A., Chaikina, M. V, Zaikovskiy, V. I., Pichugin, V. F., Buck, V., Prymak, O., Epple, M., & Surmenev, R. A. (2013). The structure of an RF-magnetron sputter-deposited silicate-containing hydroxyapatite-based coating investigated by high-resolution techniques. Surface and Coatings Technology, 218, 39–46.

[120] Amaravathy, P., Sathyanarayanan, S., Sowndarya, S., & Rajendran, N. (2014). Bioactive HA/TiO2 coating on magnesium alloy for biomedical applications. Ceramics International, 40(5), 6617–6630.

[121] Rojaee, R., Fathi, M., Raeissi, K., & Sharifnabi, A. (2014). Biodegradation assessment of nanostructured fluoridated hydroxyapatite coatings on biomedical grade magnesium alloy. Ceramics International, 40(9), 15149–15158 .

[122] Dorozhkin, S. V. (2015). Calcium orthophosphate bioceramics. Ceramics International, 41(10), 13913–13966.

[123] Kattimani, V. S., Kondaka, S., & Lingamaneni, K. P. (2016). Hydroxyapatite–Past, present, and future in bone regeneration. Bone and Tissue Regeneration Insights, 7, BTRI-S36138.

[124] Teo, A. J. T., Mishra, A., Park, I., Kim, Y.-J., Park, W.-T., & Yoon, Y.-J. (2016). Polymeric biomaterials for medical implants and devices. ACS Biomaterials Science & Engineering, 2(4), 454–472.

[125] Shin, K., Acri, T., Geary, S., & Salem, A. K. (2017). Biomimetic mineralization of biomaterials using simulated body fluids for bone tissue engineering and regenerative medicine. Tissue Engineering Part A, 23(19–20), 1169–1180.

[126] Jodhani, G., & Gouma, P.-I. (2017). Flame spray pyrolysis processing to produce metastable phases of metal oxides. JOJ Material Science, 1, 1–5.

[127] Solero, G. A. G. (2017). Synthesis of nanoparticles through flame spray pyrolysis: experimental apparatus and preliminary results.

[128] Rukosuyev, M., Baqar, S., Nam, J., Yun, H., & Jun, M. B.-G. (2018). Flame-Assisted Spray Pyrolysis Using an Annular Flame Nozzle with Decoupled Velocity Control. Journal of Manufacturing and Materials Processing, 2(4), 75.

[129] Neto, P. B., Buss, L., Meierhofer, F., Meier, H. F., Fritsching, U., & Noriler, D. (2018). Combustion kinetic analysis of flame spray pyrolysis process. Chemical Engineering and Processing-Process Intensification, 129, 17–27.

[130] Furko, M., Della Bella, E., Fini, M., & Balázsi, C. (2019). Corrosion and biocompatibility examination of multi-element modified calcium phosphate bioceramic layers. Materials Science and Engineering: C, 95, 381–388.

[131] Ji, D.-D., Xu, J.-Y., Gu, X.-F., Gao, A.-G., & Zhao, Q.-M. (2019). Preparation, characterization and biocompatibility of bioactive coating on titanium by plasma electrolytic oxidation. Science of Advanced Materials, 11(10), 1411–1415 .

[132] Wang, J.-Y., Liu, Y.-C., Lin, G.-S., Chang, H.-H., Li, Y.-T., Yang, Y.-C., Matsuyama, H., Lee, B.-S., Chen, Y.-W., & Tung, K.-L. (2020). Flame-sprayed strontium-and magnesium-doped hydroxyapatite on titanium implants for osseointegration enhancement. Surface and Coatings Technology, 386, 125452.

[133] Capellato, P., Camargo, S. E. A., & Sachs, D. (2020). Biological Response to Nanosurface Modification on Metallic Biomaterials. Current Osteoporosis Reports, 1–6.

[134] Rezaei, A., Golenji, R. B., Alipour, F., Hadavi, M. M., & Mobasherpour, I. (2020). Hydroxyapatite/hydroxyapatite-magnesium double-layer coatings as potential candidates for surface modification of 316 LVM stainless steel implants. Ceramics International, 46(16), 25374–25381.

[135] Naderi, A., Zhang, B., Belgodere, J. A., Sunder, K., & Palardy, G. (2021). Improved Biocompatible, Flexible Mesh Composites for Implant Applications via Hydroxyapatite Coating with Potential for 3-Dimensional Extracellular Matrix Network and Bone Regeneration. ACS Applied Materials & Interfaces.

[136] Shunmugasundaram, M., Praveenkumar, A., Sankar, L. P., & Sivasankar, S. (2021). Effect of Tin Oxide Coatings by Spray Pyrolysis Process on Mechanical Properties of Aluminium, Brass and Mild Steel. International Journal of Vehicle Structures & Systems (IJVSS), 13(2).

[137] Liu, Z., Liu, X., & Ramakrishna, S. (2021). Surface engineering of biomaterials in orthopedic and dental implants: Strategies to improve osteointegration, bacteriostatic and bactericidal activities. Biotechnology Journal, 2000116.

[138] Madero, J. E., Li, J., Shen, K.-Y., Wojtak, J., & Axelbaum, R. L. (2021). An approach to low-temperature flame spray pyrolysis for the synthesis of temperature-sensitive materials: Application to Li1. 2Mn0. 54Ni0. 13Co0. 13O2. Applications in Energy and Combustion Science, 5, 100020 .

[139] Dasgupta, D., Pal, P., Torelli, R., Som, S., Paulson, N., Libera, J., & Stan, M. (2022). Computational fluid dynamics modeling and analysis of silica nanoparticle synthesis in a flame spray pyrolysis reactor. Combustion and Flame, 236, 111789.

[140] Shi, D., Jiang, G., & Bauer, J. (2002). The effect of structural characteristics on the in vitro bioactivity of hydroxyapatite. Journal of Biomedical Materials Research: An Official Journal of The Society for Biomaterials, The Japanese Society for Biomaterials, and The Australian Society for Biomaterials and the Korean Society for Biomaterials, 63(1), 71-78.

[141] Tartari, T., Bachmann, L., Maliza, A. G. A., Andrade, F. B., Duarte, M. A. H., & Bramante, C. M. (2016). Tissue dissolution and modifications in dentin composition by different sodium hypochlorite concentrations. Journal of Applied Oral Science, 24, 291-298.

[142] Singh, V. K., Sharma, S., Sharma, M., Sharma, N., Sharma, J., & Rai, P. K. (2019). Application of WDXRF and FT-IR for Human Tooth Analysis. Spectroscopy, 34(12), 23-32.

[143] Palmer, L. C., Newcomb, C. J., Kaltz, S. R., Spoerke, E. D., & Stupp, S. I. (2008). Biomimetic systems for hydroxyapatite mineralization inspired by bone and enamel. Chemical reviews, 108(11), 4754-4783.

[144] Bachmann, L., Diebolder, R., Hibst, R., & Zezell, D. M. (2003). Infrared absorption bands of enamel and dentin tissues from human and bovine teeth. Applied Spectroscopy Reviews, 38(1), 1-14.

[145] Mahmood, H. S., & Jawad, M. K. (2019). Investigation of Chitosan/PEO Reinforced with AgNPs for Antibacterial Activity Prepared by Solution Casting Method. Annals of Tropical Medicine and Public Health, 22, 70-82.

[146] Cui, Y., Zhao, Y., Tian, Y., Zhang, W., Lü, X., & Jiang, X. (2012). The molecular mechanism of action of bactericidal gold nanoparticles on Escherichia coli. Biomaterials, 33(7), 2327-2333.

الخلاصــــــــــة

تم في هذا العمل، تحضير طبقه من الكالسيوم فوسفيت متوافقة حيويا على عينات من الفولاذ المقاوم للصدأ واختبار إمكانية استخدامها كغرسات طبية بطبقات متوافقة مع جسم الإنسان. تقلل هذه الطلاءات من فترة الشفاء لبناء العظام على المواد المستخدمة. تم بناء وتصميم منظومه جهاز الطلاء باللهب، تقطيع وتنظيف ركائز من الفولاذ لمقاوم للصدأ وترسيب الأغشيه بتقنية الطلاء باللهب وكذالك تم التحكم بخصائص الأغشيه المرسبه عن طريق عدة متغيرات (النسبه بين المكونات ، المسافه بين مصدر اللهب والقاعده)، فحص الأغشيه المرسبه بأستخدام عدة تقنيات (الاشعة السينية، مطياف الأشعة تحت الحمراء ، المجهر الإلكتروني لمسح الانبعاث الميداني ،مطياف تشتت الطاقه بالأشعه السينيه واختبار الطبقات المترسبه بغمرها بمحلول محاكي لجسم الانسان لمراقبة نمو الطبقات (الكالسيوم فوسفيت) على الاغنشيه المرسبه ودراسة النشاط المضاد للبكتريا للطبقات المحضره .

تم في هذا البحث تحضير طبقات من الكالسيوم فوسفيت بنسب مختلفة (1.4 ، 1.5 ، 1.65 ، 1.8 ، 1.9) ومسافات مختلفة عن فوهة اللهب (2,3,4,5,6 سم) باستخدام عملية الطلاء باللهب على الركيزة على بعد 3 سم من فتحة فوهة اللهب .   أظهرت فحوصات حيود الأشعه السينيه العديد من القمم التي تطابق التركيب البلوري لفوسفات الكالسيوم. ظهرت قمم إضافية لركيزة الفولاذ المقاوم للصدأ في جميع العينات. هنالك اختلافات صغيرة في مواضع القمم بسبب إجهاد الشبكة بسبب التباين في حجم البلورة. من الواضح ايضا ان شدة القمم زادت عند النسبة 1.65 وافضلها عند المسافة 3 سم.   من ناحية أخرى ، يتناقص عرض القمم لنفس العينة مما يشير إلى ارتفاع مستوى التبلور ونمو حجم البلورة.

اظهرت فحوصات مطياف الأشعة تحت الحمراء أن العينات احتوت على أيونات كربونات ذات أشرطة تظهر في 1412.42 و 1082.69 و 805.81 cm^{-1} للمركبات العضوية للغاز المستخدم في عملية الترسيب. بالإضافة إلى ذلك ،ظهرت نطاقات الهيدروكسيد في 3400، 1640.69، 6450.17 cm^{-1} ، وهي مطابقة لجزيئات الماء الممتصة على سطح العينات. تم إثبات أن حزم الكربونات ذات كثافة أعلى مقارنة بنطاقات الفوسفات التي تشير إلى وجود نسبة عالية من الكربونات في جميع العينات. كانت قمم الفوسفات هي الأكثر وضوحًا في العينة المحضرة بـنسبة 1.65 ومسافة 3سم مقارنة بالعينات الأخرى.

اظهر فحص المجهر الإلكتروني ان العينة المميزة والواضحة عند النسبة 1.65 ومسافة 3 سم والتي تكون ذات مسامية عالية و تحوي تراكيب نانوية مميزة.

وتم تحليل العناصر بأستخدام مطياف تشتت الطاقة للأشعة السينية وبين ظهور عناصر الاساسية لتركيب فوسفات الكالسيوم. تم غمر العينات في سائل الجسم المحاكي لجسم الإنسان لفحص التوافق الحيوي ، حيث أظهرت الاختبارات أن نسبة فوسفات الكالسيوم البالغة 1,65 هي النسبة المناسبة والمتوافقة حيوياً في جسم الإنسان. أظهرت اختبارات النشاط المضاد للبكتيريا باستخدام تقنية قرص الانتشار. على سطح الوسط الزرعي ، لاحظنا انتشار بكتريا الإشريكية القولونية على كامل الوسط عدا بعض المناطق حول بعض العينات.

يمكن اعتبار الطريقة المستخدمة كطريقة واعدة لاستخدامها في طلاء الزوارع الطبية بطريقة بسيطة بدل الطرق التقليدية المعقدة التي تحتاج الى تقنيات عالية.

جمهورية العراق

وزارة التعليم العالي والبحث العلمي

جامعة كربلاء/ كلية العلوم

قسم الفيزياء

إنشاء منظومة اللهب لتحضير طبقة متوافقة حيوياً من فوسفات الكالسيوم في الزوارع الطبية

من قبل

نبأ محمد عبد الرحيم

بكالوريوس علوم في الفيزياء 2019

إشراف

أ. د. محمد عبد الحر

أ. د. فاضل خدام فليفل

2022 م

1443هـ